DOE/NASA/0006-2
NASA CR-168195

DETERMINATION OF HYDROGEN PERMEABILITY IN COMMERCIAL AND MODIFIED SUPERALLOYS

S. BHATTACHARYYA AND W. PETERMAN

IIT Research Institute
10 West 35 Street
Chicago, Illinois 60616

May 1983

Prepared for

NATIONAL AERONAUTICS AND SPACE ADMINISTRATION
Lewis Research Center
Under Contract DEN3-6

for

U.S. DEPARTMENT OF ENERGY
Office of Transportation Programs
Under Interagency Agreement DE-A-101-77CS51040

DOE/NASA/0006-2
NASA CR-168195

DETERMINATION OF HYDROGEN PERMEABILITY IN COMMERCIAL AND MODIFIED SUPERALLOYS

S. Bhattacharyya and W. Peterman

IIT Research Institute
10 West 35 Street
Chicago, Illinois 60616

May 1983

Prepared for

NATIONAL AERONAUTICS AND SPACE ADMINISTRATION
Lewis Research Center
Under Contract DEN3-6

for
U.S. DEPARTMENT OF ENERGY
Office of Transportation Programs
Under Interagency Agreement DE-A-101-77CS51040

TABLE OF CONTENTS

LIST OF TABLES

LIST OF TABLES (cont.)

LIST OF FIGURES

LIST OF FIGURES (cont.)

SUMMARY

This report, NASA CR-168195, under Contract DEN3-6 summarizes the results of hydrogen permeability measurements on several iron- and cobalt-base alloys as well as on two long-range ordered alloys over the range of 705° to 870°C (1300° to 1600°F). The test alloys included wrought alloys N-155, IN 800, A-286, 19-9DL, and 19-9DL modifications with aluminum, niobium, and misch metal. In addition, XF-818, CRM-6D, SA-F11, and HS-31 were evaluated. Two wrought long-range ordered alloys, Ni_3Al and $(Fe,Ni)_3(V,Al)$ were also evaluated. All tests were conducted at 20.7 MPa pressure in either pure and/or 1% CO_2-doped H_2 for test periods as long as 133 h. Detailed analyses were conducted to determine the relative permeability rankings of these alloys and the effect of doping, exit surface oxidation, specimen design variations, and test duration on permeability coefficient, and permeation activation energies were determined. The two long-range ordered alloys had the lowest permeability coefficients in pure H_2 when compared with the eight commercial alloys and their modifications. With CO_2 doping, significant decrease in permeability was observed in the commercial alloys--no doped tests were conducted with the long-range ordered alloys.

INTRODUCTION

An automotive Stirling Engine development program under the joint efforts of the Department of Energy and NASA-Lewis Research Center will employ high-pressure hydrogen as the working fluid. Advantages of the Stirling engine include the potential for high fuel efficiency, multiple fuel capability, low pollution, and low noise. To achieve these operating charactistics, the Stirling engine will operate near 820°C under 15 MPa hydrogen pressure.

Containment of the working fluid (H_2) during the high temperature-pressure operation is essential to the acceptance of the Stirling engine as an alternative to the internal combustion engine. Most commercial alloys are extremely permeable to pure hydrogen at high temperatures. In an Interim Report to NASA-Lewis, NASA CR-165209,[1] the permeability of uncoated and coated superalloys was evaluated which showed that in pure H_2 the permeabilities of the commercial alloys for heater head and heater head tubing applications were too high for effective containment. Between refilling, the charged hydrogen must be contained effectively for 175 h of operation at 820°C and 21 MPa pressure. Doping of hydrogen with CO_2, along with exit side oxidation, was evaluated to decrease permeability.

This report, NASA CR-168195, under Contract DEN3-6, extends and completes the work reported earlier in NASA CR-165209 (Interim Report). In this report doped H_2 as well as pure H_2 was used with selected wrought and cast alloys, some of modified chemistries, in particular with several modifications of 19-9DL base composition. In addition, two long-range ordered (LRO) alloys, Ni_3Al and $(Fe,Ni)_3(V,Al)$, were tested in pure hydrogen. Permeability testing was conducted in a test facility specially designed and built by IITRI to operate at up to 20.7 MPa pressure and 1200°C temperature. Table 1 summarizes the major features of the various tasks and includes Task I for comparison, details of which are given in Interim Report NASA CR-165209.

MATERIALS AND EXPERIMENTAL PROCEDURE

Materials

Test Materials and Code

The test materials represented both cast and wrought alloys for heater head and tubing application, respectively. Except for the long-range ordered alloys, all the other base alloys are commercially available. Seven iron-nickel base alloys and two cobalt-base alloys, and several alloys with modified chemistries (supplied by NASA) were used in the study. The only nickel-base alloy used is the LRO alloy Ni_3Al; the other LRO alloy is $(Fe,Ni)_3(V,Al)$. Both the LROs were specially prepared by Oak Ridge National Laboratory (ORNL), Oak Ridge, TN. The alloys and their codes are given in Table 2.

The chemical compositions of the eight commercial alloys are given in Table 3, and those of the modified 19-9DL alloys are shown in Table 4. Table 5 shows the chemical composition of standard HS-31 used in Task IX along with XF-818, CRM-6D, and SA-F11, whose standard analyses are given in Table 3.

Material Microstructure

All the wrought commercial alloys had a primarily single-phase austenitic structure with varying amounts of carbides, depending on the carbon level. The cast alloys were used in the as-cast condition where the structure was single-phase austenite with significant amounts of dendritic second phase. In XF-818 and SA-F11, the dendritic second phase contained large amounts of carbides and borides. In CRM-6D the structure showed mainly carbide in the dendrites. Because of the high Mn level, there was significant porosity in this alloy structure. Typical microstructures of the eight commercial wrought and cast alloys were shown in Reference 1.

The six modified 19-9DL alloy structures were evaluated optically, and SEM/EDX analyses of selected samples were made. These microstructures are shown in Figs. 1 to 4. The unmodified as-received 19-9DL showed an equiaxed structure (Fig. 1a) with some large primary carbides and uniformly distributed particles of a finer phase in the matrix. The larger carbides appeared blocky and well outlined at high magnifications ($M_{23}C_6$ and M_6C) and were thought to be remnants of primary carbides which did not dissolve during the heat treatment.

In the 19-9DL alloy modifications coded CA and CB, the 9% Ni content of 19-9DL was increased by 2 1/2%, and 0.5% and 1% Al were added to CA and CB modifications, respectively. Alloy code CA (Fig. 1b) showed larger elongated grains with many elongated irregular-shaped grain boundary (gb) carbides which were surrounded by clusters of finer carbides. Some gb's displayed only a thin continuous layer of carbides; a very fine phase was also present in the matrix. The modification code CB (Fig. 1c) showed a much finer grain structure than CA. Blocky, outlined carbides appeared to have a bigger average size and higher volume percent. At a higher magnification in SEM, the contrast between modification codes CA and CB may be noted in Figs. 1d and e, respectively. EDX analyses of the carbides showed that the brighter particles were rich in Nb and Ti, and the light gray carbide showed mainly Fe and Cr with small amounts of Ni, Nb, and Mo.

Modification codes CD and CE of 19-9DL consisted of the additions of 2.5% Ni and 2% Nb in code CD alloy and additions of 5% Ni and 5% Nb in code CE alloy. Figure 2a shows a 125X optical photomicrograph of modification CD. Grains were less elongated than the code CA alloy, and the size is intermediate between modifications CA and CB. Grain-boundary carbides were well-defined and of irregular shape. Blocky carbides along gb's and in their vicinity comprised a significant volume fraction. Figures 2b and c show SEM details; an EDX analysis indicated that the brighter carbide particles contained high Nb and some Ti, and gb carbides were rich in Fe and Cr.

Alloy modification CE (5% Ni, 5% Nb) exhibited a more equiaxed grain structure than CD (Fig. 3a). All the carbides appeared as clusters of small outlined particles located mostly at gb or gb junctions. The matrix contained a very fine, uniformly distributed phase that was visible only at higher magnifications. Clusters of carbides observed in modification CE had two types of carbide particles: (a) scripted and outlined particles, and (b) clearly outlined particles which were separated from one another. Figures 3b and c showed typical areas with highly contrasted carbides on a uniform background. EDX analysis showed that the scripted phase contained Fe and Cr with small amounts of Nb and Ni. Blocky, rectangular-shaped particles were very rich in Nb (Fig. 3d) with small amounts of Ti, Cr, Fe, and Ni.

Modification codes CF and CG contained the addition of 2.5% Ni in both the alloys along with 0.1% and 0.3% misch metal, respectively. A comparison

of Figs. 4a and c indicates that both the alloy modifications had similar elongated grain structure with modification CG showing a little finer grain structure. Both the modifications contained relatively finer, rounded carbides at the gb's as well as in the matrix phase (Figs. 4b and d). EDX of the larger carbides from modification CG showed mainly Nb with some Ti, and little Fe and Ni. The carbides from modification CF were finer, and EDX analysis invariably contained significant contribution of the matrix phase.

Four commercial alloys, namely, XF-818, CRM-6D, SA-F11, and HS-31, evaluated and reported earlier in NASA CR-165209, were supplied by NASA. These alloys were evaluated in Task IX, and the microstructures were analyzed optically as well as with SEM/EDX. Figures 5a and b show the dendritic structure and interdendritic carbides at two magnifications. In Fig. 5b, the solid-looking carbide (A) differs from the lamellar carbide (B) which was richer in Mo while the solid-looking carbide had a higher Cr. Figures 5c and d show the Mo and Cr X-ray maps of the respective carbides.

Figure 6a shows the dendrites of XF-818 to be somewhat smaller than those of CRM-6D shown in Fig. 5a. The interdendritic carbides were lamellar as well as scripted (Fig. 6b) with a significant Mo concentration (Fig. 6c).

The SA-F11 microstructure revealed dendrites (Fig. 7a) that were somewhat smaller than those of XF-818 and more disconnected. Consequently, interdendritic spaces displayed high connectivity and a fine lamellar carbide product (Fig. 7b). The carbide-bearing areas were found to be richer in W and Cr as compared to the matrix.

Figure 7c shows a low-magnification microstructure of HS-31, a cobalt-base alloy. With a higher content of high melting elements (W, Ta, Cr, etc.) and higher carbon content, the matrix consists of cobalt-rich solid solution fcc structure with both matrix and gb carbides. In Fig. 7d, the microstructure consisted of a large M_7C_3 particle and gb $M_{23}C_6$ in a fcc matrix. EDX examination showed that both types of carbides were rich in Cr and/or W.

The Ni_3Al structure of uniform single phase, having polygonized large grains with twinning, is shown optically in Fig. 8a and in backscattered SEM in Fig. 8b. Polishing and etching have created relief in the grain pattern clearly seen in both figures.

The $(Fe,Ni)_3(V,Al)$ structure is much more complex as shown in Figs. 8c and d for optical and SEM (backscattered) photomicrographs, respectively. The grain size is much finer with a very large quantity of second-phase particles distributed on a twinned matrix phase in the form of segregated bands.

Figures 9a and b show the distribution and nature of the second phase in $(Fe,Ni)_3(V,Al)$. An optical photomicrograph is shown in Fig. 9c for comparison with the SEM photos in Figs. 9a and b. The particles are regular-shaped and faceted, similar to γ'particles of the nickel superalloy system. Several elongated particles are seen (arrow on Fig. 9a). The EDX spectra of the faceted and elongated particles, very similar in chemical composition, are shown in Fig. 9d. A semiquantitative analysis of the matrix shows the following composition (%): Ni 45.8, Fe 30.1, V 23.0, Ti 0.41, and Al 0.60. A similar analysis of the elongated particles indicated the following (%): Ni 46.3, Fe 29.4, V 22.2, Ti 0.53, Al 1.2. The similarity in composition is to be noted, and a significant contribution from the background matrix phase might have contributed to it.

Experimental Procedure

Specimen Design

Figure 10 shows the different specimen designs used in this study. Most of the tests were conducted with a 4-hole design as shown in Fig. 10(e). In NASA permeability tests,[2-4] tubular specimens with 0.81 mm wall thickness were used. In order to simulate similar material thickness and at the same time avoid membrane deformation or rupture, the multi-cavity design of Fig. 10(e) was used in Tasks VII, VIII, and IX, as indicated in Table 1. Effect of specimen design on permeability measurement is discussed in more detail in Appendix A.

Test Equipment and Procedure

Permeability measurements were made in a specially designed test facility for operation at 20.7 MPa and temperatures up to 1200°C. A schematic diagram of the test system is shown in Fig. 11. The system consists of a balanced pressure design in which the hydrogen pressure in the internal unit is balanced by nitrogen pressure in the annulus between the permeability unit and

the outer pressure vessel. The equipment internal arrangement details are shown in Fig. 12.

The specimen and the top specimen holder are assembled under a force of 17.8 kN at room temperature outside the permeability test facility. This assembly is maintained under pressure with a clamping device during incorporation into the test unit. Subsequently, the clamping pressure is maintained by the adjustable spring loading assembly at the top of the test vessel. The collecting chamber is then attached, and the exit side seal arrangement is checked to see if there is a good cold seal. This is determined if the vacuum reaches 17 Pa or less. If the initial seal appears to be adequate, the assembly is heated to the highest temperature in the testing sequence, usually 870°C, and held at that temperature under vacuum overnight prior to permeability measurements.

At the beginning of a permeability test at the desired test temperature, the output side seal leak rate is checked at atmospheric pressure by isolating the collecting chamber from the vacuum pump. A good seal will show less than 0.3 Pa/min increase in pressure. If the leak rate is acceptable, the jacket is pressurized with nitrogen (very slowly to preserve the delicate specimen seals) to 20.7 MPa with a vacuum maintained on both the entrance and exit surfaces. At full pressure, the temperature is allowed to stabilize. The collecting chamber is isolated, and the nitrogen leak rate test begins. The results are recorded on a strip chart for approximately 1 h. This test provides the baseline leak rate correction for permeability measurements. At the end of the leak rate test, the collecting chamber is evacuated to the initial value at the beginning of the leak rate test (usually less than 1.5 Pa). High purity hydrogen in the case of a pure hydrogen test, or doped hydrogen (usually 1% CO_2) in the case of a doped hydrogen test, is introduced to the inlet side of the specimen to begin the permeability tests. The collecting chamber is isolated again, and H_2 permeation is monitored by the thermistor gauge for the duration of the test (usually 5 h).

If the pen on the strip chart goes off scale, the collecting chamber is evacuated and then isolated again to give additional "series" of tests in the test day. By the end of the first series, the permeability is usually at a steady state.

For multiple temperature tests, both sides of the test sample were evacuated following the permeability test. The temperature was then reset to the temperature selected for the subsequent day's test. The specimen was again held overnight at the selected test temperature prior to the next test. In most cases, multiple temperature tests were conducted without cooling to room temperature. Temperature range was 705°-870°C. It was common practice to conduct the test at each temperature in a decreasing temperature sequence because the specimen initially seals better at the higher temperatures.

Prior to permeability tests, the collecting chamber thermistor gauge was calibrated for both hydrogen and nitrogen by injecting known volumes of the respective gases into the chamber. This procedure was repeated several times with different volumes in order to obtain two calibration curves as shown in Fig. 13. These calibration curves convert millivolt output of the thermistor gauge directly into volumes of hydrogen and nitrogen at the chamber temperature (kept at a constant above-room temperature with a tape heater), which are then converted to H_2 and N_2 volumes at standard pressure and temperature.

Since the hydrogen permeation thermistor gauge trace consists of millivolt output due to both the nitrogen "leak" and to the hydrogen permeating through the sample, the nitrogen trace was subtracted from the hydrogen permeation trace, as shown in Fig. 14. This difference (Δ) provided a third plot of millivolt output versus time due to hydrogen permeation alone, converted to a plot of ml of hydrogen (STP) versus time using the calibration curves shown in Fig. 13. A typical final plot of hydrogen permeation versus time for a typical test is shown in Fig. 15.

An excellent seal between the top specimen holder and the specimen groove was obtained by applying successively finer lapping compounds between the mismatched angle groove interface (holder 70°, specimen 60°), and by rotating the top specimen holder around the compound filled groove of the fixed specimen. The bottom seal is created by using a graphoil gasket between the flat bottom of the specimen and the raised seal surface on the bottom specimen holder. The bottom seal surface consists of a series of concentric grooves on a flat plateau 10 mm in diameter (the same as the diameter of the groove seal).

Summary Data of Test Parameters

A total of 55 tests were conducted in Tasks VII, VIII, IX, and X, as outlined in Table 1. These tests are analyzed in the next section and compared with data from 21 tests conducted under Task I and reported earlier.[1] Complete test parameters of the 55 tests are given in Tables 6, 7, 8, and 9 for Tasks VII, VIII, IX, and X, respectively.

Calculations of Permeability, Diffusivity, and Solubility

Assuming diffusion of hydrogen atoms through an isotropic structure at these high temperatures to be the principal rate-controlling process, hydrogen flow can be expressed thus:

$$j_t = \Phi \frac{A}{\Delta x} (p_i^{1/2} - p_o^{1/2}) \qquad (1)$$

where j_t = hydrogen flux normal to the surface of the specimen, $cm^3\ s^{-1}$

Φ = permeability coefficient, $cm^3\ cm^{-1}\ s^{-1}\ MPa^{-1/2}$

A = specimen area, cm^2

Δx = specimen thickness, cm

p_i, p_o = input and output H_2 pressure, respectively, MPa

Under steady-state condition,

$$J_t = \frac{DA}{\Delta x} (C_o - C_i) \qquad (2)$$

where C_o and C_i are the solute (H) concentrations at the output and input surfaces, respectively.

With diffusion as the rate-controlling step and assuming ideal behavior as a monoatomic gas:

$$C = Kp^{1/2} \qquad (3)$$

where C = hydrogen (solute) concentration

K = solubility constant

p = external hydrogen pressure

Combining Eqs. 2 and 3,

$$j_t = \frac{DKA}{\Delta x}(p_o^{1/2} - p_i^{1/2}) \tag{4}$$

From Eqs. 4 and 1, we obtain

$$\Phi = DK \tag{5}$$

If the output pressure of hydrogen, p_o, is very much less than the input pressure, p_i, such that $p_o^{1/2}$ is negligible when p_i is 20.7 MPa, as is the case in study, then

$$j_t = \Phi \frac{A}{\Delta x} p_i^{1/2} \tag{6}$$

The "lag time," θ_L--the intercept which the steady-state portion of the curve makes with the time axis, as shown in Fig. 15--is related to the diffusion term (D) for this system according to the equation:

$$\theta_L = \frac{\Delta x^2}{6D} \tag{7}$$

Thus, for each test two independent measurements were made to obtain separately, j_t and θ_L; and from Eqs. 6 and 7, independent values of Φ and D were determined. Then using Eq. 5, K, the solubility constant, was derived which thus incorporated and possibly enhanced the existing uncertainties in the independent measurements of Φ and D.

The diffusion and solubility terms, D and K, respectively, may be assumed to obey an Arrhenius-type relationship with temperature:

$$D = D_o \exp(-Q_D/RT) \tag{8}$$

$$K = K_o \exp(-Q_K/RT) \tag{9}$$

where D_o and K_o are the respective pre-exponential diffusion and solubility-related terms, and Q_D and Q_K are the respective activation energies.

Using Eq. 5, one then obtains:

$$Q = Q_0 \exp(-Q_\phi/RT) \quad (10)$$

$$\text{when } \phi_0 = D_0K_0 \quad (11)$$

$$\text{and } Q_\phi = Q_D + Q_K \quad (12)$$

EXPERIMENTAL RESULTS

All the experimental data on permeability are grouped separately for each task. The permeability data from all these tasks are compared and analyzed in the following manner:

Effect of Alloy Composition on Permeability in Pure H_2

- Modified 19-9DL Alloys (Task VIII)
- XF-818, CRM-6D, SA-F11, and HS-31 Alloys (Task IX)
- Two Long-Range Ordered Alloys, Ni_3Al and $(Fe,Ni)_3(V,Al)$ (Task X)

Effect of Oxides on Permeability

- Effect of Doped H_2 on Permeability

  Comparison of Doped vs. Pure H_2 on 19-9DL, N-155, IN 800 and A-286 (Tasks VII vs. I)

  Comparison of Doped H_2 on 19-9DL (Std.) vs. Modified 19-9DL (Tasks VII vs. VIII)

  Comparison of Doped vs. Pure H_2 on XF-818, CRM-6D, SA-F11, and HS-31 (Task IX).

- Effect of Exit Oxide

Effect of Alloy Composition on Permeability in Pure H_2

Modified 19-9DL Alloys (Task VIII)

Table 10 summarizes the permeability results for the six 19-9DL modified alloys at four different test temperatures. At each temperature, the alloys may be ranked as shown in Table 11. It is to be noted, however, that the ϕ values do not necessarily vary widely between the least and highest permeable alloys at each temperature as shown below:

Temp., °C	Least Permeability			Highest Permeability		
	Alloy (Code)		ϕ (in E-06 units[a])	Alloy (Code)		ϕ (in E-06 units)
705	2.5Ni, 0.5Al	(CA)	14.2	2.5Ni, 1.0Al	(CB)	35.0
760	2.5Ni, 2.0Nb	(CD)	37.2	5.0Ni, 5.0Nb	(CE)	79.2
815	2.5Ni, 0.3MM[b]	(CG)	65.4	5.0Ni, 5.0Nb	(CE)	172
870	2.5Ni, 0.5Al	(CA)	138	2.5Ni, 2.0Nb	(CD)	211

[a]Unit = $cm^3\ cm^{-1}\ s^{-1}\ MPa^{-1/2}$.

[b]MM = misch metal.

In Fig. 16, the ϕ values for each alloy are plotted as the reciprocal of absolute temperature. The vertical bars positioned at respective temperatures (the ones for the doped H_2 are included for later analysis) indicate the range of measured ϕ values for the different alloys. The lengths of the bars indicate that the lowest and highest permeability values are within one order of magnitude. The average ϕ values for all the six alloy modifications shown in Fig. 16 are plotted in Fig. 17 against 1/T, and a regression line was fitted to obtain the following results:

Item	Permeability Statistical Analysis Parameter			
	Y-intercept ($\ln \phi_o$)	Slope (Q/R)	Activation Energy (Q), kJ/mole	Correlation Coefficient (R^2)
All 6 alloy modifications of 19-9DL in pure H_2	3.59	-13.9	116	1.00

In the earlier study (Task I, NASA CR-165209), the activation energy of standard alloy 19-9DL in pure H_2 was noted as 80 kJ/mole. There are, however, several differences between the test parameters of Tasks I and VIII, in addition to alloy chemistry modifications, and these are as follows:

Item	Specimen Design			Activation Energy (Q), kJ/mole
	Thickness, mm	Area, mm^2	Exit Surface	
Task VIII	0.82	17.6	Oxidized	116
Task I	5.50	78.5	Not oxidized	80

The higher activation energy for permeation observed in Task VIII is thus a combined effect of alloy modifications and surface oxidation effect, as well as specimen area and thickness factors.

In permeability tests, a test series was usually started at the highest temperature and consisted of so-called "sequences." Thus, the four temperatures of 870°, 815°, 760°, and 705°C tested on four different days were called:

870°C - Sequence 1
815°C - Sequence 2
760°C - Sequence 3
705°C - Sequence 4

Sequence 1 at 870°C started without any preoxidation of the exit surface. In pure H_2 tests, no oxidation occurred on the entrance side throughout the tests, but in doped H_2, the 870°C and the subsequent lower temperature tests developed oxides of increasing thickness on the entry side. For various reasons, a sequence step may have been immediately rerun for a separate reading, which was given the same sequence number with a suffix "b" added to it, the first one being indicated with suffix "a."

Figure 17 analyzes the average permeability coefficient of the six modified 19-9DL alloys, whereas the data for 19-9CL alloy modification CE with 5% Ni and 5% Nb are plotted in Fig. 18. The fitted regression line had a slope of -13.2 (Q = 110 kJ/mole) with R^2 = 0.94, indicating a good correlation of the data with temperature.

XF-818, CRM-6D, SA-F11, and HS-31 Alloys (Task IX)

Permeability data in pure H_2 obtained at four temperatures, 870° to 705°C, are summarized in Table 12. Permeability values increased with temperature with XF-818 showing the highest values at 705° and 870°C; the rankings at the highest and lowest temperatures are as follows:

Rank	870°C		705°C	
	Alloy	ϕ, E-06 units[a]	Alloy	ϕ, E-06 units
Least	SA-F11	93.5	HS-31	9.50
↓	CRM-6D	107	CRM-6D	10.1
	HS-31	112	SA-F11	13.0
Highest	XF-818	173	XF-818	39.0

[a]Unit = $cm^3\ cm^{-1}\ s^{-1}\ MPa^{-1/2}$.

Permeation activation energy for each alloy was obtained by plotting ln ϕ vs. 1/T, as shown in Fig. 19. Linear regression lines were fitted through the data to obtain the terms ϕ_o and Q, the activation energy as well as the multiple correlation coefficient, R^2 given below:

	Permeability Statistical Analysis Parameters			
Alloy	Y-intercept (ln ϕ_o)	Slope (Q/R)	Activation Energy (Q), kJ/mole	Correlation Coefficient (R^2)
XF-818	10.4	-10.3	86	0.99
CRM-6D	7.68	-19.0	158	0.82
SA-F11	2.76	-13.8	115	0.99
HS-31	5.13	-16.2	135	0.98

Except for CRM-6D, the R^2 values ranged from 0.95 to 1.00 indicating a good fit of the data.

Earlier in Task I, the three iron-nickel base cast alloys, XF-818, CRM-6D, and SA-F11, and the cobalt-base alloy, low carbon Stellite 6B (LC), all in standard commercial compositions, were evaluated in pure H_2 in the 650°-815°C temperature range. These results were summarized in NASA CR-165209.

In Fig. 19, the permeation data for Task I alloys were plotted to compare with those of Task IX alloys. The slopes indicated that the activation energies of the Task I alloys were all lower; in other words, the Task IX alloys had an improved performance, as shown below:

Alloys	Activation Energy (Q_ϕ) in Pure H_2, kJ/mole	
	Task IX	Task I
XF-818	86	52
CRM-6D	158	69
SA-F11	115	49
HS-31	135	34

The observed significant improvements in lowered permeability at the higher temperatures (above 760°C) and higher activation energies may be due to a combination of the following:

1. Differences in the alloy chemistry/treatment in XF-818, CRM-6D, and SA-F11.
2. Significant compositional differences between standard Stellite 6B (LC) and HS-31; e.g., W: 3.84 (6B) and 7.5 (HS-31); Ni: 2.08 (6B) and 10.5 (HS-31); Cr: 29.2 (6B) and 25.5 (HS-31).
3. Task I alloys were tested without any exit surface oxidation whereas Task IX alloy specimen exit surfaces were oxidized.

Two Long-Range Ordered Alloys (Task X)

The two long-range ordered alloys (LROs) selected for evaluation were supplied by Oak Ridge National Laboratory (ORNL), with the following chemistry and sample numbers:

Alloy Type	Sample No.	Code	Test No.
Ni_3Al	IC-50-B	IC	112
$(Fe,Ni)_3(V,Al)$	LRO-55-F	LR	113

The test samples were supplied in the form of flat disks, 2.78 and 2.36 mm thick for Ni_3Al and $(Fe,Ni)_3(V,Al)$, respectively, conforming to specimen design shown in Fig. [illegible]). According to Dr. C. T. Liu of ORNL, the order-disorder temperature (T_c) of Ni_3Al exceeds 1350°C and that for $(Fe,Ni)_3(V,Al)$ is above 900°C. Below these temperatures, these ordered wrought alloys are strong and tend to increase in strength with temperature. While strength data for the two tested alloys were not available, typical strength values of three

other LROs shown in Fig. 20[5] indicate progressive increase in yield strength with temperature up to the critical ordering temperature (T_c) while those of Hastelloy X and 316 SS continually decreased.

Both the alloys were tested in pure H_2 with exit surfaces not oxidized between sequences. The permeability data are summarized in Table 13. The permeability values in both the alloys are extremely low, and at a temperature as high as 815°C the permeation values were less than 1.0 E-06 $cm^3\ cm^{-1}\ s^{-1}\ MPa^{-1/2}$, the reliable detection limit of the apparatus of the present design. These ϕ values are plotted in Fig. 21 as ln ϕ vs. 1/T, where T is the test temperature in the absolute scale.

In Fig. 21, two lines were fitted by linear correlation, one for Ni_3Al and the other for $(Fe,Ni)_3(V,Al)$ and the following parameters were obtained:

	Permeability Statistical Analysis Parameters			
Alloy	Y-Intercept (ln ϕ_o)	Slope (Q/R)	Activation Energy (Q), kJ/mole	Correlation Coefficient (R^2)
Ni_3Al	7.39	-21.4	178	0.83
$(Fe,Ni)_3(V,Al)$	7.33	-21.8	177	0.80

The significantly low permeability coefficients of the two LRO alloys in pure H_2--compared at a typical temperature of 815°C with the standard and modified alloys tested in Tasks I, VIII, and IX--are given below:

Task	Alloys	Permeability Coefficient (ϕ) in Pure H_2 at 815°C, in E-06 units[a]	Activation Energy (Q), kJ/mole
I	N-155, IN 800, 19-9DL, A-286, CRM-6D, XF-818, SA-F11, 6B (LC)	19-43	34-80
VIII	Six modified 19-9DL alloys	100 (avg)	116 (avg)
IX	XF-818, CRM-6D, SA-F11, HS-31	50-120	86-158
X	Ni_3Al; $(Fe,Ni)_3(V,Al)$	4.5; 3.2	178 (for both alloys)

[a]Unit = $cm^3\ cm^{-1}\ s^{-1}\ MPa^{-1/2}$

The two LRO alloys exhibited at least an order of magnitude lower permeability in pure H_2 when compared with Task I commercial alloys tested under similar specimen design (solid disks) with no exit surface oxidation. In both Tasks VIII and IX, similar multicavity specimen design was used with exit surface oxidation and these results are thus not directly comparable with Task X data.

Because the Task X permeability values were mostly beyond the reliable detection limit of the present equipment design, a large scatter in the data is reflected in the low R^2 values of about 0.80. With equipment modification to improve detection of lower permeability coefficients and additional tests, the LRO permeabilities could be more accurately determined.

Effect of Oxides on Permeability

Effect of Doped H_2 Permeability

Comparison of Doped vs. Pure H_2 in Four Alloys (Task VII vs. I). The four commercial alloys evaluated were N-155, 19-9DL, IN 800, and A-286. A total of 20 tests were conducted in H_2 doped with 1% CO_2. The same four alloys were evaluated in pure H_2 in Task I. The similarities and differences between Tasks VII and I test conditions are summarized in Table 1. All the Task VII permeability data are summarized in Tables 14 and 15.

Figure 22 plots the pure H_2 (Task I) and doped H_2 (Task VII) permeability coefficients of four alloys. Significant differences in alloy response to doping are evident. The related activation energies are summarized below:

Alloy	Environment	Permeation Activation Energy, kJ/mole
N-155	Doped H_2	63
	Pure H_2	79
19-9DL	Doped H_2	199
	Pure H_2	80
IN 800	Doped H_2	69
	Pure H_2	78
A-286	Doped H_2	139
	Pure H_2	60

In 19-9DL and A-286 alloys, doping increased permeation activation energy more than twofold, but did not affect permeation activation energy in N-155 and IN 800 significantly. The high activation energies for 19-9DL and A-286 are reflected in the higher permeability values at 760°C and higher temperatures and in the much lower values at temperatures lower than 760°C. Because Task I tests were conducted to 650°C and not above 815°C, permeability coefficients at two intermediate temperatures, 705° and 815°C, were calculated from Fig. 22 and these are summarized in Table 16.

Table 16 data show that at 815°C in these short duration tests (total time 20 to 25 h) H_2 permeation appears to be unaffected by the development of oxide on the entrance surface due to doping with permeation coefficient remaining larger than in pure H_2. Later, longer term tests showed that with an effective buildup of oxide, ϕ decreased significantly (see Appendix A).

Comparison of Modified 19-9DL vs. Standard 19-9DL Alloys in Doped Hydrogen (Task VIII vs. VII). In Task VIII, six modifications of 19-9DL alloys were evaluated at four different temperatures in 1% CO_2-doped H_2, tested in duplicate. All the permeability data are summarized in Table 17. Using the average of the duplicate ϕ values, the six different alloy modifications are ranked in Table 18.

Table 18 data show that an alloy which is of lower permeability at one temperature does not necessarily retain the relative lower permeability property at the higher temperature. For example, the least and highest permeabilities were as follows:

Temp, °C	Least	Highest
705	2.5Ni, 1.0Al	2.5Ni, 0.3MM[a]
760	5.0Ni, 5.0Nb	2.5Ni, 0.1MM
815	5.0Ni, 5.0Nb	2.5Ni, 0.1MM
870	2.5Ni, 0.5Al	5.0Ni, 5.0Nb

[a]MM = misch metal.

It is to be noted, however, that at 870°C, exit surface oxides were not created by oxidation. At all other temperatures, a deliberate high temperature oxidation in air built up an oxide layer which would have affected permeability differently depending on the relative oxidation properties and the amount of alloying elements present in the composition.

Table 18 data also show that the 2.5Ni addition with 1.0Al performed better than most other alloys at all four temperatures. A similar good performance was noted for the 2.5Ni, 2.0Nb modification.

While the ranking shows the different permeation tendencies between the alloy modifications, in absolute terms, the ϕ values did not differ significantly, as indicated below:

Temp., °C	Least Permeability		Highest Permeability	
	Alloy (Code)	ϕ (in E-06 units[a])	Alloy (Code)	ϕ (in E-06 units)
705	2.5Ni, 1.0Al	3.15	2.5Ni, 0.3MM[b]	17.7
760	5.0Ni, 5.0Nb	10.7	2.5Ni, 0.1MM	34.2
815	5.0Ni, 5.0Nb	18.1	2.5Ni, 0.1MM	58.6
870	2.5Ni, 0.5Al	107	5.0Ni, 5.0Nb	187

[a] Unit = $cm^3\ cm^{-1}\ s^{-1}\ MPa^{-1/2}$.

[b] MM = misch metal.

The average ϕ values in doped H_2 (from Table 18) are plotted vs. 1/T and shown in Fig. 16. The six alloy ranges of ϕ values and the average ϕ values are indicated on Fig. 16. The permeability coefficient difference between the least and highest values is less than one order of magnitude with the largest difference, a factor of 6 (doped, 705°C) decreasing with temperature to about a factor of 2 (doped, 870°C).

In order to determine the effect of doped environment in producing dynamic oxidation (and maintaining an oxide layer) and thereby decreasing permeation by affecting H_2 activation energy, the average ϕ values of all six modifications were analyzed versus 1/T through statistical correlation. The statistically fitted lines for the doped values have the following parameters.

Item	Permeability Statistical Analysis Parameters			
	Y-intercept ($\ln \phi_o$)	Slope (Q/R)	Activation Energy (Q), kJ/mole	Correlation Coefficient (R^2)
All six 19-9DL alloys (mod.) in doped H_2	7.74	-19.1	159	0.96
All six 19-9DL alloys (mod.) in pure H_2	3.59	-13.9	116	1.00

The lower activation energy in pure H_2 is one indication of the barrier put up by the dynamic oxidation process created by doping. However, in these short duration tests, the reduction in ϕ due to inside oxide was small; the effect of the outer oxide with time, therefore, was investigated and is discussed in Appendix A.

A comparative analysis of Tasks VIII, VII, and I permeability data in pure and doped H_2 indicates the following:

- Task VIII vs. VII (average of all 6 modifications). In doped H_2, there appears to be no difference in permeation activation energy between the standard 19-9DL (161 kJ/mole) and the average of all 6 alloy modifications (159 kJ/mole)
- Task VII vs. Task I (19-9DL, std.). In the standard alloy, doping appears to double the activation energy for permeation (80 to 161 kJ/mole)
- Task VIII, Doped vs. Pure H_2 (6 alloy average). This comparison shows that doping increases Q for H_2 permeation by 40% and decreases permeability proportionately.

Comparison of Doped vs. Pure H_2 on XF-818, CRM-6D, SA-F11, and HS-31 (Task IX). The test data of the cast alloys, XF-818, CRM-6D, SA-F11, and HS-31 in pure and doped H_2 are summarized in Table 19. The test data in pure H_2 have been analyzed earlier and compared with pure H_2 permeability of these four cast alloys conducted under Task I.

In the doped H_2 tests, the effect of CO_2 dopant in building up surface oxide on the entry side was further evaluated by running an additional sequence 5 test at 870°C, in essence repeating sequence 1 test after 15 h of testing at the three lower temperatures. These data are indicated at the lower row of Table 19.

Table 19 data show that, in all cases, permeability was larger in pure H_2 than in doped-H_2; the significance depending on alloy composition and temperature. The largest differences were noted in CRM-6D as noted below:

Sequence	Temp., °C	Ratio of ϕ_{pure}/ϕ_{doped}
1	870	1.8
2	815	2.6
3	760	8.7
4	705	7.7

The data indicate a signific .t increase in the ratio at the lower temperatures in CRM-6D. In other words, 1% CO_2 was more effective in reducing permeation in CRM-6D at 760° and 705°C. A similar behavior was noted earlier in alloys A-286 and 19-9DL (see Fig. 22). The behavior of the three other alloys was somewhat different as seen below:

Sequence	Temp., °C	Ratio of ϕ_{pure}/ϕ_{doped}		
		XF-818	HS-31	SA-FII
1	870	1.3	1.1	1.1
2	815	2.2	0.9	2.4
3	760	2.4	1.3	1.5
4	705	3.0	1.1	2.3

These data show that a trend exists in the effectiveness of doping action, which increases at the lower temperatures. HS-31 showed the least effectiveness of doping at all four temperatures, while XF-818 showed a trend similar to that shown for CRM-6D.

A comparison of 870°C doped H_2 data for sequences 1 and 5 indicates the time effect; sequence 1 was completed in 5 h, and sequence 5 between 20 and 25 h. However, in sequence 1, the exit surface had no oxide present. A comparison of Table 19 data indicates that ϕ decreases with time in the following manner.

Alloy	Ratio of $\phi(25\ h)/\phi(5\ h)^a$
XF-818	0.85
HS-31	0.78
SA-F11	0.28
CRM-6D	0.19

[a]At 870°C, 1% CO_2-doped H_2.

Similar time effects were observed in extended tests conducted with IN 800 and 19-9DL, and these data are analyzed in Appendix A.

The complex relative behavior of doping and time effects in reducing permeability of these alloys as well as in 19-9DL and A-286, analyzed earlier, must be in some way related to the chemistry as well as to the nature of oxide scale with preferential element concentration and protective scale formation at different temperatures. Generally, chromium and manganese enrichment has been noted. Complex spinels form, and their stability in hydrogen at high temperature dictates permeability. In a significant study, Schuon and Misencik[4] have suggested that in CO_2-doped H_2, reduction in H_2 permeability was more strongly affected by the minor elements of the alloy chemistry--Al, Ti, Nb, or La. In the alloys investigated, Al and Ti were present in 19-9DL (std. as well as mod.), IN 800, and A-286 while Nb+Ta were present in XF-818, and CRM-6D, as well as in 19-9DL (mod.) alloys. Extended tests with 19-9DL (mod.) alloys had indicated a time effect as shown in Appendix A.

The ϕ values from Table 19 were plotted as a function of temperature as shown in Fig. 23. Linear regression lines were drawn through the data and the related statistical data are summarized in Table 20.

The order of activation energies in doped and pure H_2 is as follows:

Rank	Doped H_2	Pure H_2	Remarks
1	CRM-6D	CRM-6D	Highest Q
2	HS-31	HS-31	↓
3	SA-F11	SA-F11	
4	XF-818	XF-818	Lowest Q

It may be seen that under doping, the relative ranking did not change.

Effect of Exit Oxide

That an exit surface oxide can cause a significant decrease in permeation was shown by Schuon and Misencik.[4] In NASA rig tests, the tube outside is heated in air and develops a continually increasing thickness of oxide. To simulate this effect, several tests were conducted with IN 800 where, for a period, the exit surface was left in vacuum/H_2 and later exposed to air at high temperatures. The results of these tests are summarized in Table 21 and shown in Figs. 24, 25, and 26.

During the first 25 to 30 h exposure, there was no exit surface oxidation and permeability decreased very slowly as shown in Figs. 24 to 26. However, after 25 h, the sample exit surface was exposed to air at the high temperatures between test sequences and a rapid drop in permeability took place in the following period both with doped H_2 (entrance side oxides present) and with pure H_2.

On each test sequence, several series of measurements were made and these are shown in the form of a bar depicting the overall range values in Figs. 24 to 26. The sequence numbers are indicated, and estimated curves are drawn to indicate the rate of decrease. It is quite apparent that once exit surface oxidation had started, the rate of decrease accelerated.

The effect of exit oxide on permeability in cast alloys can be determined by comparing the activation energies of pure H_2 tests of Task IX with those of Task I. The Q values are as follows:

Alloys	Q, kJ/mole	
	Task IX	Task I
XF-818	86	52
CRM-6D	158	69
SA-F11	115	49
HS-31	135	34

The much higher Q for values Task IX tests indicate the oxide development on the exit side; the Task I tests were conducted without the exit sides exposed to air. However, the specimen designs were different for Tasks IX and I, whereas those for IN 800 alloys tested in Task VII were identical. These

IN 800 tests clearly indicated that exit surface oxide buildup can contribute significantly to reduction of permeability and behaves in a manner similar to entry side oxide buildup caused by H_2 doping.

SUMMARY OF RESULTS

Hydrogen permeability was measured on several iron- and cobalt-base alloys as well as on two long-range ordered alloys over the temperature range 705° to 870°C. Both pure and 1% CO_2-doped hydrogen were used. The results of this study are summarized below:

- Significant reduction in hydrogen permeability occurred with 1% CO_2 doping of hydrogen.
- Hydrogen permeabilities in 1% CO_2-doped H_2 at 815°C in the wrought alloys were 38 to 68 E-06 cm^3 cm^{-1} s^{-1} $MPa^{-1/2}$, and in the cast alloys 9 to 60 E-06 cm^3 cm^{-1} s^{-1} $MPa^{-1/2}$.
- To decrease permeability to 1.0 E-06 cm^3 cm^{-1} s^{-1} $MPa^{-1/2}$, it was necessary to expose 19-9DL alloys to time periods of 70-80 h in doped H_2. Combined with exit surface oxidation, permeability in doped H_2 could be reduced to 1.0 E-06 level in about 50 h.
- 19-9DL composition modifications did not contribute to a significant reduction in permeability when compared with standard 19-9DL alloy in pure H_2. However, doping was more effective in reducing permeability in the modified 19-9DL alloys when compared with pure H_2 permeability.
- Hydrogen permeability of pure H_2 in the long-range ordered alloys (LROs) Ni_3Al and $(Fe,Ni)_3(V,Al)$ were much lower than those in all the commercial and modified wrought and cast alloys, and values of 1.4 to 4.3 E-06 cm^3 cm^{-1} s^{-1} $MPa^{-1/2}$ were possible in pure H_2 at 815°C; doped H_2 tests were not conducted. The pure hydrogen permeation activation energies of the LROs were about 180 kJ/mole as compared to 40-80 kJ/mole for the commercial alloys.

ACKNOWLEDGMENTS

This study was sponsored by NASA-Lewis Research Center, Cleveland, Ohio, under Contract DEN3-6, for the United States Department of Energy, Office of Transportation Programs. The test alloys were supplied by NASA-Lewis and Oak Ridge National Laboratory (ORNL), Oak Ridge, Tennessee. We are grateful to S. Schuon and J. Stephens of NASA-Lewis and C. T. Liu (ORNL) for their help and encouragement. At IITRI, W. Peterman conducted the tests, and T. Todner and S. C. Agarwal helped in the metallographic activities.

REFERENCES

1. S. Bhattacharyya, E. J. Vesely, Jr., and V. L. Hill, "Determination of Hydrogen Permeability in Uncoated and Coated Superalloys," Interim Report, NASA CR-165209, January 1981, NASA-Lewis Research Center, Cleveland, Ohio 44135.

2. John A. Misencik, "Evaluation of Candidate Stirling Engine Heater Tube Alloys for 1000 Hours at 760°C," NASA TM-81578, November 1980, NASA-Lewis Research Center, Cleveland, Ohio 44135.

3. Joseph R. Stephens, "Characterization of Stirling Engine Materials," presented at Automotive Technology Development Contractor Coordination Meeting, Dearborn, Michigan, Oct. 25-28, 1982.

4. Susan R. Schuon and John A. Misencik, "Effect of Oxide Films on Hydrogen Permeability of Candidate Stirling Heater Head Tube Alloys," NASA TM-82824, prepared for 110th AIME Annual Meeting, Chicago, IL, Feb. 22-26, 1981.

5. C. T. Liu, "Physical Metallurgy and Mechanical Properties of Ductile Long-Range Ordered Alloys $(Fe,Ni,Co)_3V$," to be published in the International Metals Review, 1984.

APPENDIX A

EFFECT OF TEST CONDITIONS

Specimen Design Effect

The different specimen designs used in this program are shown in Fig. 10. The initial specimen design, Fig. 10(a), used in Tasks I to III was modified to the newer design, Fig. 10(b), with the sample in both designs having the same 10 mm diameter permeation area. The specimen thicknesses of 5.1 to 6.4 mm were chosen to reduce stresses due to 20.7 MPa H_2 pressure at 870°C.

In Task VII, the possibility of specimen thickness affecting permeability in doped H_2 was considered in analyzing IITRI and NASA data. NASA tests were performed using tubes with a 0.81 mm wall thickness. The thinnest monolithic specimen possible in IITRI tests under standard design is 2.5 mm, as shown in Fig. 10(c). A pressure of 20.7 MPa over the 78.5 mm^2 area could cause a large stress of 40 MPa to develop in the specimen, and at the higher temperatures, the specimen may deform. Membrane thickness equal to NASA tube wall thickness was obtained using multicavity specimens. Single cavity, 4-cavity, and 7-cavity modifications were tried, as shown in Figs. 10(d) and (e). Typical photographs of multicavity specimens are shown in Fig. 27.

A 7-cavity specimen worked well, but the overlapping high stresses caused observable deformation as shown in Fig. 28a. The outline of the depressed region containing the seven cavities appears lighter in the photograph. SEM photomicrographs of the base of the holes on the exit side (tensile side) show cracks as may be seen in Fig. 28b. Because of these problems with the 7-cavity specimen design, all remaining tests under Tasks VII, VIII, and IX were made with the 4-cavity design; Task X tests were made with Fig. 10(b) design--a thin, monolithic specimen.

A membrane area of significant amount is needed to obtain sufficient hydrogen permeation, and typical results comparing single-cavity, 4-, and 7-cavity specimen are given in Table 22. The data show that a single-cavity specimen had such a low membrane area (4.4 mm^2) that total hydrogen collection was inadequate for permeability calculation. Both 4- and 7-cavity designs with areas of 17.6 and 31.2 mm^2 were sufficient for adequate measurement.

However, for reasons of high stresses, the 7-cavity design was not used, as mentioned earlier.

Effect of Time and Test Sequence on Permeability

In all the standard tests, the specimen permeability measurements lasted for a duration of about 5 h at each temperature. In doped-H_2, such a short time did not allow for the development of a significant thickness of oxide on the inlet surface (relative to membrane thickness of about 0.8 mm), and the effect of longer test duration was evaluated in several tests, some of which are indicated below:

Alloy	Specimen Design (Fig. 10)	Test Area, mm^2	Test Thickness, mm	Test Sequence	Cumulative Time, h	Permeability, E-06 units[a]
IN 800 (test 68)	(b)	78.5	5.9	1-16 17-27[b]	81.8 51.1	80 to 40 40 to 3
IN 800 (test 75)	(d)	4.4	0.76	1-5 6-10[b]	28.5 26.7	10 to 7 7 to <1
19-9DL (2.5Ni,1.0Al) (test 111)	(d)	17.6	0.76	1-5[b]	46.0	140 to 24

[a]Unit = $cm^3\ cm^{-1}\ s^{-1}\ MPa^{-1/2}$.

[b]Specimen exit surface oxidized between sequences. All tests conducted at 815°C in 1% CO_2-doped H_2.

Alloy IN 800 permeability results for 133 h using thick, monolithic specimens (test 68) are plotted in Fig. 29. Out of a total of 27 sequences (average 5 h) evaluated, typical values of 8 sequences were plotted and an estimated curve was drawn through these data points. During the first 16 sequences, the exit surface was not oxidized and only a factor of 2 decrease in permeability occurred solely due to entrance side oxide buildup from doping. However, beyond about 80 to 90 h, a combination of entry side oxide buildup with external oxide formation reduced permeability by an order of magnitude.

Alloy IN 800 permeability data for 55 h using a single-cavity thin specimen (test 75) are plotted in Fig. 30. The trend shows that a very large drop in permeability occurred with time.

One standard and two modified 19-9DL alloy coupons were tested in several sequences for as long as 60 h, and these data are given in Table 23. Test 111 data plotted in Fig. 31 show a sharp decrease in permeability with time in 1% CO_2-doped H_2 with exit surface oxidation.

The results indicate that doped hydrogen will slowly build up an internal oxide layer which will decrease permeability. However, it takes anywhere from 70 to 80 h to build up enough oxide thickness (the thickness is also relative to the wall thickness) which may also be a function of alloy chemistry, temperature, and related parameters. However, if sufficient time is allowed, both internal oxide due to doping and external oxidation can effectively reduce permeability coefficient to a level below 1.0 E-06 $cm^3\ cm^{-1}\ s^{-1}\ MPa^{-1/2}$ at 815°C--the desired goal for adequate retention of hydrogen for a 6-month refilling interval in an operating automobile.

TABLE 1. MAJOR FEATURES OF VARIOUS TASKS

Task I	Task VII	Task VIII	Task IX	Task X
		Alloy (Code)		
N-155 (A)	N-155 (A)	19-9DL		Long-range ordered alloys, Ni_3Al and $(Fe,Ni)_3(V,Al)$
IN 800 (B)	IN 800 (B)	+ 2 1/2Ni, 1/2Al (CA)		
19-9DL (C)	19-9DL (C)	+ 2 1/2Ni, 1Al (CB)		
A-286 (D)	A-286 (D)	+ 2 1/2Ni, 2Nb (CD)		
		+ 5Ni, 5Nb (CE)		
		+ 2 1/2Ni, 0.1 MM* (CF)		
		+ 2 1/2Ni, 0.3 MM* (CG)		
		*MM = Misch Metal		
CRM-6D (J)			CRM 6D (JA)	
6B LC (K)			SA-F11 (PA)	
SA-F11 (P)			XF-818 (QA)	
XF-818 (Q)			HS-31 (RA)	
		Environment		
	Doped, 1% CO_2	Doped, 1% CO_2	Doped, 1% CO_2	
	Doped, 1% CO			
Pure H_2	Pure H_2	Pure H_2	Pure H_2	Pure H_2
		Specimen Design		
Solid, thick	Solid, thick			Solid, thin
	Solid, thin			
	With holes (1, 4, 7)	4 holes	4 holes	
		Temperatures, °C		
650	705	705	705	705
705	760	760	760	760
760	815	815	815	815
815	870	870	870	870
		Exit-Surface Oxidation		
None	Yes, on some tests.	All tests	All tests	None
		Time, h		
5 to 25	5 to 133	5 to 60	5 to 25	5 to 25

TABLE 2. MATERIALS AND CODES

Iron-Base Alloys

Wrought Alloys		Task I Cast Alloys	
Code	Alloy	Code	Alloy
A	N-155	J	CRM-6D
B	IN 800	P	SA-F11
C	19-9DL	G	XF-818
D	A-286		

Modified Iron-Base Alloys

Wrought 19-9DL		Task IX Cast Alloys	
Code	Modifications	Code	Alloy
CA	2.5Ni + 0.5Al	JA	CRM-6D
CB	2.5Ni + 1.0Al	PA	SA-F11
CD	2.5Ni + 2.0Nb	GA	XF-818
CE	5.0Ni + 5.0Nb		
CF	2.5Ni + 0.1 Misch metal		
CG	2.5Ni + 0.3 Misch metal		

Cobalt-Base Alloys

Code	Alloy
K	LC 6B (low carbon alloy 6B)
RA	HS-31

Long-Range Ordered Alloys

Code	Alloy
IC	Ni_3Al, No. IC-50-B
LR[b]	$(Fe,Ni)_3(V,Al)$, No. LRO-55-F

TABLE 3. COMMERCIAL SUPERALLOYS[a]

Element	SA-F11[b]	XF-818[b]	CRM-6D[b]	Stellite 6B	N-155	19-9DL	IN 800	A-286
C	0.64	0.23	1.11	0.41	0.11	0.31	0.08	0.05
Si	0.60	0.38	0.48	0.36	0.83	0.80	0.14	0.16
Mn	0.49	0.17	3.30	1.04	1.20	0.83	0.71	0.11
P	0.038	0.009	0.016	0.031	-	0.023	0.022	0.015
S	0.018	0.015	0.020	0.008	-	0.01	0.007	0.008
Fe	48.36	53.28	63.46	2.05	28.82	66.28	47.25	55.76
Ni	17.12	18.80	5.45	2.08	20.04	9.28	30.10	25.05
Cr	23.17	18.21	22.67	29.21	21.60	18.86	20.38	14.16
Mo	0.15	7.30	1.14	0.90	2.90	1.48	-	1.72
W	7.39	-	1.05	3.84	3.05	1.30	-	-
Nb + Ta	-	0.42	1.20	-	1.10	0.42	-	-
Ti	-	-	-	-	-	0.20	0.30	2.35
Co	-	-	-	59.80	20.50	-	-	-
Other	0.44B	1.1B	-	-	0.15N	0.13Cu	0.31Al	0.16Al 0.004B

Heat treatment: Plates heated to the following temperatures in argon and air cooled:

N-155 - 1182°C (2160°F) Incoloy 800 - 1121°C (2050°F)

A-286 - 982°C (1800°F) 19-9DL - 977°C (1790°F)

[a]Composition in weight percent.

[b]Cast alloys.

TABLE 4. MODIFIED 19-9DL ALLOYS

Alloy Identification Code	Modifications
C	Unmodified[a]
CA	2.5Ni + 0.5Al
CB	2.5Ni + 1.0Al
CC[b]	5.0Ni + 1.0Al
CD	2.5Ni + 2.0Nb
CE	5.0Ni + 5.0Nb
CF	2.5Ni + 0.1 Misch metal
CG	2.5Ni + 0.3 Misch metal

[a]Unmodified 19-9DL was also tested. Modifications are in addition to the following standard composition.

C 0.30, Mn 1.10, Si 0.60, Cr 19, Ni 9.0, Mo 1.25, W 1.20, Nb 0.40, Ti 0.30, Fe - balance.

[b]Alloy available but not tested.

TABLE 5. NOMINAL CHEMICAL ANALYSIS OF HS-31[a]

Element	Composition, wt%
C	0.5
Si	0.75
Mn	0.75
P	0.04[b]
S	0.04[b]
Fe	2.0[b]
Ni	10.5
Cr	25.5
W	7.5
Co	54

[a]Standard alloy analysis.

[b]Maximum.

TABLE 6. DATA ON MATERIALS, TEMPERATURE, AND OTHER PERMEABILITY TEST PARAMETERS FOR N-155, IN 800, 19-9DL, AND A-286 ALLOYS (TASK VII)

Test No.	Sample No.[a]	Specimen Design[b]	Area, mm^2	Thick-ness, mm	Temp., °C	Test Sequence[c]	Cumulative Time, h
			Alloy N-155				
56	A400[d]	(b)	78.5	6.1	650	4	20.4
					705	3	15.4
					760	2	10.1
					815	1	5.1
					815	5	24.9
59	A403	(b)	78.5	6.1	650	4	17.1
					650	8	36.8
					705	3	12.1
					705	5	21.7
					760	2	7.4
					760	6	26.0
					815	1	2.6
					815	7	31.6
					870	9	42.1
61	A405	(b)	78.5	6.1	870	1	4.4
63	A407	(b)	78.5	6.1	705	1	5.2
					705	6	17.8
					760	2	7.8
					815	3	11.3
					870	4	14.0
					870	7	22.7
76	A500	(d)	4.4	.89	705[e]	4	14.6
					760[e]	3	10.5
					815[e]	2	6.9
					870	1	3.5
					870[e]	5	17.8
77	A501	(e)	31.2	.86	705[e]	4	17.1
					760[e]	3	12.0
					815[e]	2	6.8
					870	1	3.1
					870[e]	5	22.3
			IN 800				
64	B405	(b)	78.5	6.3	705	1	5.3
					760	2	10.4
					815	3	13.9
					870	4	18.4
65a	B406	(b)	78.5	6.3	870	1	4.0

TABLE 6 (cont.)

Test No.	Sample No.[a]	Specimen Design[b]	Area, mm^2	Thickness, mm	Temp., °C	Test Sequence[c]	Cumulative Time, h
65b	B407	(b)	78.5	6.2	705	4	17.2
					760	3	13.7
					815	2	8.4
					870	1	4.9
					870	5	21.2
66	B408	(b)	78.5	6.2	705	4	19.2
					705	6	29.7
					705	8	40.6
					705	10	49.4
					760	3	13.4
					815	2	7.9
					870	1	2.7
					870	5	24.9
					870	7	35.1
					870	9	45.5
					870	11	54.9
67	B400	(b)	78.5	5.9	705	1	4.7
					705	5	25.9
					705	7	36.3
					705	9	46.3
					705	11	57.2
					705	15	77.4
					760	2	10.1
					760	14	72.6
					815	3	15.3
					815	13	67.4
					870	4	20.4
					870	6	31.1
					870	8	41.1
					870	10	51.1
					870	12	62.2
68	B401	(b)	78.5	5.9	815	1	4.0
					815	2	9.3
					815	3	14.4
					815	4	19.6
					815	5	24.9
					815	6	30.5
					815	7	35.4
					815	8	40.5
					815	9	45.3
					815	10	50.8
					815	11	55.8
					815	12	61.1
					815	13	66.3

TABLE 6 (cont.)

Test No.	Sample No.[a]	Specimen Design[b]	Area, mm^2	Thickness, mm	Temp., °C	Test Sequence[c]	Cumulative Time, h
68					815	14	71.6
					815	15	76.6
					815	16[e]	81.8
					815	17[e]	87.5
					815	18[e]	93.1
					815	19[e]	98.2
					815	20[e]	102.2
					815	21[e]	106.1
					815	22[e]	109.8
					815	23[e]	114.1
					815	24[e]	119.5
					815	25[e]	123.8
					815	26[e]	128.2
					815	27[e]	132.9
59	B402	(b)	78.5	5.9	815	1[e]	4.1
					815	2[e]	10.4
					815	3[e]	15.7
					815	4[e]	20.7
71	B403	(b)	78.5	6.0	815	1	5.2
					815	2	12.1
					815	3	17.1
					815	4	22.2
					815	5	27.2
					815	6[e]	32.4
					815	7[e]	37.8
					815	8[e]	43.5
					815	9[e]	48.9
					815	10[e]	55.1
72	B409	(c)	78.5	2.7	815	1	3.0
					815	2	7.0
					815	3	12.0
					815	4	17.5
					815	5	22.6
					815	6[e]	27.8
					815	7[e]	33.0
					815	8[e]	38.2
					815	9[e]	43.5
					815	10[e]	48.5
					815	11[e]	53.5
73	B410	(c)	78.5	2.6	815	1	3.6
					815	2	8.9
					815	3	13.9
					815	4	19.5
					815	5	24.6

TABLE 6 (cont.)

Test No.	Sample No.[a]	Specimen Design[b]	Area, mm^2	Thickness, mm	Temp., °C	Test Sequence[c]	Cumulative Time, h
73					815	6[e]	29.6
					815	7[e]	34.6
					815	8[e]	39.9
					815	9[e]	45.2
					815	10[e]	50.4
74	B500	(d)	2.01	.76	815	1	4.3
					815	2	9.5
					815	3	15.0
					815	4	20.4
					815	5	25.9
					815	6[e]	30.9
					815	7[e]	34.2
					815	8[e]	37.2
					815	9[e]	42.2
					815	10[e]	47.1
75	B501	(d)	4.38	.89	815	1	5.0
					815	2	10.2
					815	3	15.7
					815	4	21.0
					815	5	28.5
					815	6[e]	33.8
					815	7[e]	39.0
					815	8[e]	44.1
					815	9[e]	50.1
					815	10[e]	55.2
			19-9DL				
78	C500	(e) 7 hole	31.2	.86	705	4[e]	20.0
					760	3[e]	13.2
					815	2[e]	8.1
					870	1	3.0
80	C501	(e) 4 hole	17.6	.86	705	4[e]	20.4
					760	3[e]	15.3
					815	2[e]	10.1
					870	1	5.0
			A-286				
79	D500	(e) 7 hole	31.2	.86	705	4[e]	20.8
					760	3[e]	16.2
					815	2[e]	10.7
					870	1	5.0

TABLE 6 (concl.)

Test No.	Sample No.[a]	Specimen Design[b]	Area, mm^2	Thickness, mm	Temp., °C	Test Sequence[c]	Cumulative Time, h
82	D501	(e) 4 hole	17.6	.84	705	4[e]	21.1
					760	3[e]	15.7
					815	2[e]	10.4
					870	1	5.4

[a]For alloy codes see Table 2.

[b]See Fig. 10 for identification of (b), (c), (d), and (e).

[c]Tests started with sequence 1.

[d]Except for tests 67, 66, and 73, all tests were conducted with H_2 + 1% CO_2. Tests 67 and 66 were done with H_2 + 1% CO and test 73 in pure H_2.

[e]Oxidation of exit side between test sequences in each test; sequence 1 did not have the exit side oxidized.

TABLE 7. DATA ON MATERIALS, TEMPERATURE, AND OTHER PERMEABILITY TEST PARAMETERS FOR 19-9DL MODIFIED ALLOYS (TASK VIII)

Test No.	Sample No.	Thickness,[a] mm	Temp., °C	Test Sequence	Cumulative Time, h
81	CA500[b]	0.91	870	1	5.4
			815	2	10.5
			760	3	16.0
			705	4	16.0
83	CB500[b]	0.76	870	1	5.2
			815	2	10.6
			760	3	15.7
			705	4	21.0
85	CB501[c]	0.79	870	1	5.0
			815	2	8.6
			760	3	13.6
			705	4	18.7
			705	4'	23.7
86	CA501[c]	0.84	870	1	5.2
			870	1'	5.0
			815	2	10.1
			760	3	15.5
			705	4	20.8
87	CD500[b]	0.85	870	1	5.3
			815	2	10.7
			760	3	15.9
			705	4	21.2
			870	5	25.9
88	CA502[b]	0.83	870	1	5.1
			815	2	10.0
			760	3	15.0
			705	4	19.8
			870	5	24.8
89	CB502[b]	0.81	870	1	3.6
			815	2	8.9
			760	3	14.4
			705	4	19.5
			870	5	24.3
90	CD502[b]	0.83	870	1	5.0
			815	2	10.2
			760	3	15.3
			705	4	20.4
			870	5	26.0

TABLE 7 (cont.)

Test No.	Sample No.	Thickness,[a] mm	Temp., °C	Test Sequence	Cumulative Time, h
91	CE500[b]	0.80	870	1	5.1
			815	2	10.3
			760	3	15.4
			705	4	20.4
			870	5	24.8
92	CG500[b]	0.81	870	1	5.0
			815	2	10.0
			760	3	15.2
			705	4	20.2
			870	5	24.2
93	CF500[b]	0.84	870	1	5.3
			815	2	10.3
			760	3	15.3
			705	4	20.3
			870	5	25.3
94	CE502[b]	0.81	870	1	5.2
			815	2	10.2
			760	3	15.2
			705	4	20.2
			870	5	25.2
95	CF502[b]	0.84	870	1	5.2
			815	2	10.2
			760	3	15.3
			705	4	20.3
			870	5	25.4
96	CD501[c]	0.84	870	1	5.0
			815	2	10.2
			760	3	15.2
			705	4	20.2
97	CE501[c]	0.81	870	1	5.0
			815	2	10.0
			760	3	15.0
			705	4	20.0

TABLE 7 (concl.)

Test No.	Sample No.	Thickness,[a] mm	Temp., °C	Test Sequence	Cumulative Time, h
98	CF501[c]	0.85	870	1	5.0
			815	2	10.4
			760	3	15.4
			705	4	20.5
99	CG501[c]	0.84	870	1	5.0
			815	2	10.0
			760	3	15.0
			705	4	20.2
100	CG502[b]	0.84	870	1	5.0
			815	2	10.0
			760	3	15.0
			705	4	20.4
			870	5	25.4
			870	6	30.4
			815	7	35.5
			760	8	40.0
109	C501[b]	0.84	815	3 to 8	60
110	CD500[b]	0.85	815	1 to 5	52
111	CB500[b]	0.76	815	1 to 5	47

[a]Four-hole specimens were used in all these tests with an area of 17.6 mm^2, Fig. 10(e). Exit surfaces were oxidized after test sequence 1.

[b]The environment was H_2 + 1% CO_2. For alloy sample code see Table 2.

[c]The environment was pure H_2.

TABLE 8. DATA ON MATERIALS, TEMPERATURE, AND OTHER PERMEABILITY TEST PARAMETERS FOR XF-818, HS-31, SA-F11, AND CRM-6D ALLOYS (TASK IX)

Test No.	Sample No.	Thickness,[a] mm	Temp., °C	Test Sequence	Cumulative Time, h
101	QA500[b]	0.83	870	1	5.0
			815	2	10.0
			760	3	15.0
			705	4	20.5
			870	5	25.5
102	RA500[b]	0.83	870	1	5.0
			815	2	10.3
			760	3	15.3
			705	4	20.3
			870	5	25.3
103	PA500[b]	0.86	870	1	5.0
			815	2	10.0
			760	3	15.1
			705	4	20.0
			870	5	25.0
104	JA500[b]	0.86	870	1	5.0
			815	2	9.3
			760	3	14.8
			705	4	20.0
			870	5	24.8
105	QA501[c]	0.85	870	1	5.0
			815	2	10.2
			760	3	15.4
			705	4	20.4
106	JA501[c]	0.86	870	1	5.0
			815	2	10.1
			760	3	15.3
			705	4	20.4
107	PA501[c]	0.86	870	1	5.1
			815	2	10.2
			760	3	15.2
			705	4	20.2
108	RA501[c]	0.86	870	1	5.2
			815	2	10.3
			760	3	15.8
			705	4	21.3

[a]Four-hole specimens were used in all these tests with an area of 17.6 mm^2 (Fig. 10e).

[b]The environment was H_2 + 1% CO_2. For alloy sample code, see Table 2.

[c]The environment was pure H_2. All exit surfaces were oxidized after sequence 1.

TABLE 9. DATA ON MATERIALS, TEMPERATURE, AND OTHER PERMEABILITY TEST PARAMETERS OF TWO LONG-RANGE ORDERED ALLOYS (TASK X)

Test No.	Sample No.[a]	Specimen Design[b]	Area, mm^2	Thickness, mm	Temp., °C	Test Sequence	Cumulative Time, h
112	IC400	(c)	78.5	2.78	870	1	4.9
					870	2	9.9
					875	3	14.9
					760	4	19.6
					760	5[c]	24.6
					760	6	29.6
					705	7	--
					815	8	38.7
					870	9	43.0
113	LR400	(c)	78.5	2.36	870	1	5.0
					815	2	10.0
					760	3	15.4
					705	4	20.4

[a]For alloy code, see Table 2. All tests conducted in pure H_2 without exit-side oxidation between tests.

[b]Solid flat specimen, see Fig. 10(c).

[c]Not analyzed due to high seal leak rate.

TABLE 10. PURE HYDROGEN PERMEABILITY IN SIX MODIFIED 19-9DL ALLOYS (Task VIII)

19-9DL Alloy Modification, %	Permeability Coefficient (ϕ) at Different Temperatures, cm^3 (STP) cm^{-1} s^{-1} $MPa^{-1/2}$			
	705°C (978 K)	760°C (1033 K)	815°C (1088 K)	870°C (1143 K)
2.5Ni + 0.5Al	1.42 E-05	4.27 E-05	8.56 E-05	1.38 E-04
2.5Ni + 1.0Al	3.50 E-05	6.01 E-05	9.93 E-05	1.98 E-04
2.5Ni + 2.0Nb	1.45 E-05	3.72 E-05	9.96 E-05	2.11 E-04
5.0Ni + 5.0Nb	3.02 E-05	7.29 E-05	1.72 E-04	1.92 E-04
2.5Ni + 0.1MM[a]	2.76 E-05	5.10 E-05	9.02 E-05	1.83 E-04
2.5Ni + 0.3MM[a]	1.93 E-05	4.67 E-05	6.54 E-05	1.75 E-04

Note: All Task VIII and IX tests were initiated at 870°C with the specimen exit surface in the as-machined condition. At all subsequent lower temperature levels, the exit surface of the specimen was oxidized having been left open with access to air at the test temperature for 16 to 18 h before the next test.

[a]MM = Misch metal.

TABLE 11. PURE HYDROGEN PERMEABILITY RANKING OF SIX MODIFIED 19-9DL ALLOYS (TASK VIII)

Rank	Permeability Ranking of Alloys at Different Test Temperatures			
	705°C (978 K)	760°C (1033 K)	815°C (1088 K)	870°C (1143 K)
Least	2.5Ni, 0.5Al	2.5Ni, 2.0Nb	2.5Ni, 0.3MM[a]	2.5Ni, 0.5Al
	2.5Ni, 2.0Nb	2.5Ni, 0.5Al	2.5Ni, 0.5Al	2.5Ni, 0.3MM
↓	2.5Ni, 0.3MM	2.5Ni, 0.3MM	2.5Ni, 0.1MM	2.5Ni, 0.1MM
	2.5Ni, 0.1MM	2.5Ni, 0.1MM	2.5Ni, 1.0Al	5.0Ni, 5.0Nb
	5.0Ni, 5.0Nb	2.5Ni, 1.0Al	2.5Ni, 2.0Nb	2.5Ni, 1.0Al
Highest	2.5Ni, 1.0Al	5.0Ni, 5.0Nb	5.0Ni, 5.0Nb	2.5Ni, 2.0Nb

[a]MM = Misch metal.

TABLE 12. PURE HYDROGEN PERMEABILITY IN XF-818,CRM-6D, SA-F11, AND HS-31 ALLOYS (TASK IX)

Alloy	Permeability Coefficient (ϕ) at Different Temperatures, cm^3 (STP) cm^{-1} s^{-1} $MPa^{-1/2}$			
	705°C (978 K)	760°C (1033 K)	815°C (1088 K)	870°C (1143 K)
XF-818 (Mod.)	3.90 E-05	6.95 E-05	1.23 E-04	1.73 E-04
CRM-6D (Mod.)	1.01 E-05	1.16 E-05	1.08 E-04	1.07 E-04
SA-F11 (Mod.)	1.30 E-05	2.16 E-05	5.18 E-05	9.35 E-05
HS-31 (Mod.)	9.50 E-06	3.10 E-05	5.34 E-05	1.12 E-04

TABLE 13. PURE HYDROGEN PERMEABILITY IN TWO LONG-RANGE ORDERED ALLOYS (TASK X)

Permeability Coefficient (ϕ) at Different Temperatures, cm^3 (STP) cm^{-1} s^{-1} $MPa^{-1/2}$			
870°C (1143 K)	815°C (1088 K)	760°C (1033 K)	705°C (978 K)
Alloy Ni_3Al			
Sequence 1	Sequence 3	Sequence 6	Sequence 7
1.97 E-05	1.37 E-06 (14.9 h)	1.85 E-06	5.18 E-07 (34.4 h)
1.45 E-05		2.17 E-06 (29.6 h)	
1.03 E-05 (4.9 h)[a]			
Alloy $(Fe,Ni)_3(V,Al)$			
Sequence 1	Sequence 2	Sequence 3	Sequence 4
8.62 E-06	4.32 E-06	2.50 E-07 (15.4 h)	3.06 E-07
8.27 E-06 (5.0 h)	4.25 E-06 (10.0 h)		6.28 E-07 (20.4 h)

[a]Values in parentheses indicate cumulative testing hours on specimens. Specimen exit surfaces were not oxidized between different sequences.

TABLE 14. HYDROGEN PERMEABILITY IN N-155, IN 800, 19-9DL, AND A-286 ALLOYS (TASK VII)[a]

Test No.	Alloy	H_2 Permeability at Different Test Temperatures, E-06 units[b]							
		705°C (978 K)		760°C (1033 K)		815°C (1088 K)		870°C (1143 K)	
		1% CO_2-Doped Hydrogen							
56[c]	N-155	23.4	(3)[d]	10.3	(2)	2.91	(1)		
						48.1	(5)		
59[c]	N-155	47.3	(3)	43.8	(2)	64.4	(1)	35.1	(9)
		45.2	(5)	35.8	(6)	36.7	(7)		
61	N-155							78.4	(1)
63	N-155	19.2	(1)	25.6	(2)	42.0	(3)	41.1	(7)
76	N-155	<1.1	(4)	<1.1	(3)	<1.1	(2)	32	(1)
								<1.1	(5)
77	N-155	12.8	(4)	23.1	(3)	35.8	(2)	89.8	(1)
								46.2	(5)
64	IN 800	27.1	(1)	35.3	(2)	44.5	(3)	39.1	(4)
65a	IN 800							127	(1)
65b	IN 800	42.4	(4)	35.3	(5)	85.1	(2)	102	(1)
								94.1	(5)
68	IN 800					0.98	(19)[e]		
						73.6	(9)		
69	IN 800					22.6	(2)[e]		
						28.1	(1)		
71	IN 800					1.58	(10)[e]		
						94.1	(2)		
72	IN 800					7.0	(9)[e]		
						48.3	(3)		
74	IN 800					103	(3)[e]		
						589	(8)		
75	IN 800					<1.1	(7-10)[e]		
						113	(1)		
70	19-9DL					32.4	(1)		
78	19-9DL	29.6	(4)	13.5	(3)	38.0	(2)	80.3	(1)
80	19-9DL	2.3	(4)	13.3	(3)	44.5	(2)	99.2	(1)
79	A-286	13.1	(5)	8.55	(3)	33.2	(2)	124	(1)
		5.94	(4)						
82	A-286	10.5	(4)	29.7	(3)	43.5	(2)	160	(1)

TABLE 14 (cont.)

Test No.	Alloy	H_2 Permeability at Different Test Temperatures, E-06 units[b] 705°C (978 K)		760°C (1033 K)		815°C (1088 K)		870°C (1143 K)	
				1% CO-Doped Hydrogen					
66	IN 800	18.2 29.3	(8)[e] (6)	22.3	(3)	47.7	(2)	60.6 193	(7)[e] (1)
67	IN 800	28.3 39.6	(9)[e] (5)	24.9 45.4	(2) (14	35.6 64.0	(3) (13)	73.0 96.0	(10)[e] (4)
				Pure Hydrogen					
73	IN 800					7.8 53.6	(7)[e] (1)		

[a]For test parameter details see Table 6.

[b]Unit = $cm^3\ cm^{-1}\ s^{-1}\ MPa^{-1/2}$.

[c]Two tests were made with N-155 only at 650°C with the following results:

Test 56: ϕ = 1.90 E-05 units
Test 59: ϕ = 4.68 E-05 units
2.24 E-05 units

[d]Numbers in parentheses indicate test sequence, starting with sequence 1.

[e]See Table 15 for actual values for each sequence.

TABLE 15. HYDROGEN PERMEABILITY FOR IN 800 EXPOSED FOR LONG DURATIONS

Test No.	Temp., °C (K)	H_2 Permeability at Different Sequences[a] (in E-06 units)[b]									
		Pure Hydrogen									
73	815 (1143)	53.6 (1)	40.8 (2)	33.0 (3)	29.3 (4)	40.9 (5)	36.1[c] (6)	7.8 (7)	20.6 (8)	16.2 (9)	32.9 (10)
		1% CO-Doped Hydrogen									
66	705 (978)	19.6 (4)	29.3 (6)	18.2 (8)	24.0 (10)						
	870 (1143)	19.3 (1)	74.3 (5)	60.6 (7)	84.0 (9)	87.7 (11)					
67	705 (978)	28.6 (1)	39.6 (5)	28.3 (7)	28.3 (9)	29.7 (11)	35.5 (15)				
	870 (1143)	96.0 (4)	81.7 (6)	93.5 (8)	73.0 (10)	82.8 (12)					
		1% CO_2-Doped Hydrogen									
68	815 (1088)	64.0 (1)	40.4 (2)	45.4 (3)	63.0 (4)	33.9 (5)	61.9 (6)	46.4 (7)	54.8 (8)	73.6 (9)	53.4 (10)
		72.6 (11)	42.9 (12)	45.3 (13)	31.2 (14)	68.4 (15)	34.5 (16)	30.2 (17)	7.12 (18)	0.98 (19)	11.0 (20)
		5.66 (21)	5.74 (22)	8.92 (23)	3.97 (24)	6.72 (25)	5.57 (26)	2.87 (27)			
69	815 (1088)	28.1 (1)	22.6 (2)	27.3 (3)	26.7 (4)						
71	815 (1088)	34.2 (1)	94.1 (2)	60.4 (3)	63.5 (4)	73.6 (5)	18.9[c] (6)	10.6 (7)	17.9 (8)	9.9 (9)	1.58 (10)
72	815 (1088)	24.8 (1)	47.0 (2)	48.3 (3)	45.9 (4)	46.0 (5)	14.2[c] (6)	11.1 (7)	8.05 (8)	7.02 (9)	
74	815 (1088)	169 (1)	115 (2)	103 (3)	331 (4)	160 (5)	199[c] (6)	589 (8)	462 (9)	269 (10)	
75	815 (1088)	113 (1)	40.5 (2)	17.6 (3)	8.58 (4)	6.17 (5)	1.76[c] (6)	<1.1 (7)	<1.1 (8)	<1.1 (9)	<1.1 (10)

[a]Sequence numbers are given in parentheses below the permeability values.

[b]Unit = $cm^3\ cm^{-1}\ s^{-1}\ MPa^{-1/2}$.

[c]Exit surface oxidized starting from this sequence.

TABLE 16. A COMPARISON OF PERMEABILITY OF DOPED VS. PURE H_2 IN N-155, IN 800, 19-9DL, AND A-286 ALLOYS

Alloy	Environment	H_2 Permeability Coefficient (in E-06 units)[a] 705°C (978 K)	815°C (1088 K)
N-155	Doped	22	48
	Pure	10	27
19-9DL	Doped	3.4	38
	Pure	7.2	19
IN 800	Doped	29	68
	Pure	10	23
A-286	Doped	9.2	51
	Pure	13	27

[a]Unit = $cm^3\ cm^{-1}\ s^{-1}\ MPa^{-1/2}$

TABLE 17. DOPED HYDROGEN PERMEABILITY IN SIX MODIFIED 19-9DL ALLOYS (TASK VIII)

19-9DL Alloy Modification, %	Permeability Coefficient (ϕ) at Different Temperatures, cm^3 (STP) $cm^{-1}\ s^{-1}\ MPa^{-1/2}$ 705°C (978 K)	760°C (1033 K)	815°C (1088 K)	870°C (1143 K)
2.5Ni + 0.5Al	8.28 E-06	2.81 E-05	5.36 E-05	1.01 E-04
	7.09 E-06	1.74 E-05	4.91 E-05	1.12 E-04
2.5Ni + 1.0Al	3.28 E-06	3.01 E-05	5.94 E-05	1.21 E-04
	3.02 E-06	6.72 E-06	2.46 E-05	1.70 E-04
2.5Ni + 2.0Nb	1.01 E-05	1.83 E-05	5.64 E-05	1.42 E-04
	4.52 E-06	9.45 E-06	4.21 E-05	1.42 E-04
5.0Ni + 5.0Nb	1.43 E-05	2.05 E-05	2.57 E-05	2.03 E-04
	8.40 E-07	a	1.05 E-05	1.70 E-04
2.5Ni + 0.1MM[b]	6.81 E-06	2.33 E-05	5.20 E-05	1.53 E-04
	1.70 E-05	4.50 E-05	6.52 E-05	1.82 E-04
2.5Ni + 0.3MM[b]	2.12 E-05	3.50 E-05	5.74 E-05	1.77 E-04
	1.41 E-05	3.21 E-05	4.43 E-05	1.82 E-04

[a]Seal problem.

[b]MM = Misch metal

TABLE 18. HYDROGEN PERMEABILITY RANKING OF SIX MODIFIED 19-9DL ALLOYS IN DOPED H_2 (TASK VIII)

Rank	Permeability Ranking of Alloys at Different Test Temperatures			
	705°C (978 K)	760°C (1033 K)	815°C (1088 K)	870°C (1143 K)
Least	2.5Ni, 1.0Al	5.0Ni, 5.0Nb	5.0Ni, 5.0Nb	2.5Ni, 0.5Al
	2.5Ni, 2.0Nb	2.5Ni, 2.0Nb	2.5Ni, 1.0Al	2.5Ni, 1.0Al
	5.0Ni, 5.0Nb	2.5Ni, 1.0Al	2.5Ni, 2.0Nb	2.5Ni, 2.0Nb
	2.5Ni, 0.5Al	2.5Ni, 0.5Al	2.5Ni, 0.3MM[a]	2.5Ni, 0.1MM
	2.5Ni, 0.1MM	2.5Ni, 0.3MM	2.5Ni, 0.5Al	2.5Ni, 0.3MM
Highest	2.5Ni, 0.3MM	2.5Ni, 0.1MM	2.5Ni, 0.1MM	5.0Ni, 5.0Nb

[a]MM = Misch metal.

TABLE 19. HYDROGEN PERMEABILITY IN ALLOYS XF-818, HS-31, SA-F11, AND CRM-6D IN PURE AND 1% CO_2-DOPED HYDROGEN (TASK IX)

Sequence	Test Temp., °C (K)	Environment	Permeability (ϕ), $cm^3\ cm^{-1}\ s^{-1}\ MPa^{-1/2}$			
			XF-818	HS-31	SA-F11	CRM-6D
1	870 (1143)	Doped	1.29 E-04 (101)[a]	1.04 E-04 (102)	8.16 E-05 (104)	5.80 E-05 (104)
		Pure	1.73 E-04 (105)	1.12 E-04 (108)	9.35 E-05 (107)	1.07 E-04 (106)
2	815 (1088)	Doped	5.67 E-05 (101)	5.86 E-05 (102)	2.15 E-05 (103)	4.19 E-06 (104)
		Pure	1.23 E-04 (105)	5.34 E-05 (108)	5.18 E-05 (107)	1.08 E-04 (106)
3	760 (1143)	Doped	2.90 E-05 (101)	2.37 E-05 (102)	1.48 E-05 (103)	1.34 E-05 (104)
		Pure	6.95 E-05 (105)	3.10 E-05 (108)	2.16 E-05 (107)	1.16 E-05 (106)
4	705 (978)	Doped	1.31 E-05 (101)	8.76 E-06 (102)	5.65 E-06 (103)	1.32 E-06 (104)
		Pure	3.90 E-05 (105)	9.50 E-06 (108)	1.30 E-05 (107)	1.01 E-05 (106)
5	870 (1143)	Doped	1.06 E-04 (101)	8.24 E-05 (102)	2.28 E-05 (103)	1.10 E-05 (104)

[a]Test numbers are given in parentheses.

TABLE 20. REGRESSION ANALYSIS OF PERMEABILITY COEFFICIENT FOR FOUR ALLOYS (TASK IX)

Alloy	Environment	Regression Analysis Data			
		Y-Intercept ($\ln \phi_o$)	Q/R	Q, kJ/mole	Corr. Coeff. R^2
XF-818	Doped	4.36	-15.3	127	1.00
	Pure	10.4	-10.3	86	0.99
HS-31	Doped	5.93	-17.2	143	0.99
	Pure	5.13	-16.2	135	0.98
SA-F11	Doped	5.23	-17.0	141	0.95
	Pure	2.76	-13.8	115	0.99
CRM-6D	Doped	11.2	-24.9	207	0.78
	Pure	7.68	-19.0	158	0.82

TABLE 21. EFFECT OF EXIT SURFACE OXIDATION ON PERMEABILITY FOR IN 800 AT 815°C (TASK VII)

Test No.	Specimen Design	Environment	Permeability Coefficient after Given Time, 10^{-6} cm^3 cm^{-1} s^{-1} $MPa^{-1/2}$					
			Before Exit Surface Oxidation			After Exit Surface Oxidation[a]		
			5 h	15 h	25 h	35 h	45 h	55 h
71	Thick,[b] solid	Doped H_2	80	75	65	35	15	2
72	Thin, solid	Doped H_2	40	35	30	15	5	<1
73	Thin, solid	Pure H_2	40	40	35	25	15	<1

[a]Including time before exit surface oxidation.

[b]Thick = 5.96 mm; thin = 2.62 mm.

TABLE 22. EFFECT OF SPECIMEN DESIGN ON HYDROGEN PERMEABILITY

Alloy	Specimen Design (Fig. 10)	Test Area, mm^2	Test Thickness, mm	Test Temp., °C	Test Sequence	Permeability, E-06 units[a]
N-155	(d)	4.4	0.89	705	4[b]	<1.1[c]
				760	3[b]	<1.1
				815	2[b]	<1.1
				870	1	32
				870	5[b]	<1.1
N-155	(e)	31.2	0.89	705	4[b]	13
				760	3[b]	23
				815	2[b]	36
				870	1	90
				870	5[b]	46
19-9DL	(e)	17.6	0.86	705	4[b]	3.4
				760	3[b]	13
				815	2[b]	45
				870	1	99
19-9DL	(e)	31.2	0.86	705	4[b]	30
				760	3[b]	14
				815	2[b]	38
				870	1	80

[a] Unit = $cm^3\ cm^{-1}\ s^{-1}\ MPa^{-1/2}$

[b] Specimen exit surface oxidized between sequences.

[c] Total hydrogen volume was too low for accurate detection.

TABLE 23. HYDROGEN PERMEABILITY IN 19-9DL ALLOYS EXPOSED FOR LONG DURATIONS

Test No.	Temp., C (K)	Alloy	H_2 Permeability at Different Sequences,[a] E-06 units[b]					
109	815 (1143)	Std. 19-9DL	1.47 (3)	3.64 (4)	4.02 (5)	2.43 (6)	2.65 (7)	1.58 (8)
110	815 (1143)	Mod. 19-9DL (2.5Ni + 2.0Nb)	13.6 (1)	33.6 (2)	27.7 (3)	22.2 (4)	12.8 (5)	
111	815 (1143)	Mod. 19-9DL (2.5Ni + 1.0Al)	161 (1)	11.2 (2)	78.9 (3)	24.2 (4)	16.5 (5)	

[a]Sequence numbers are given in parentheses below the permeability values.

[b]Unit = $cm^3\ cm^{-1}\ s^{-1}\ MPa^{-1/2}$.

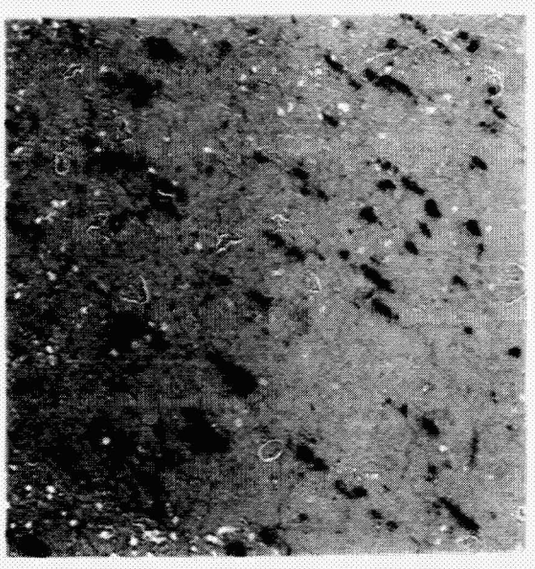

Neg. No. 53538 125X

(a)

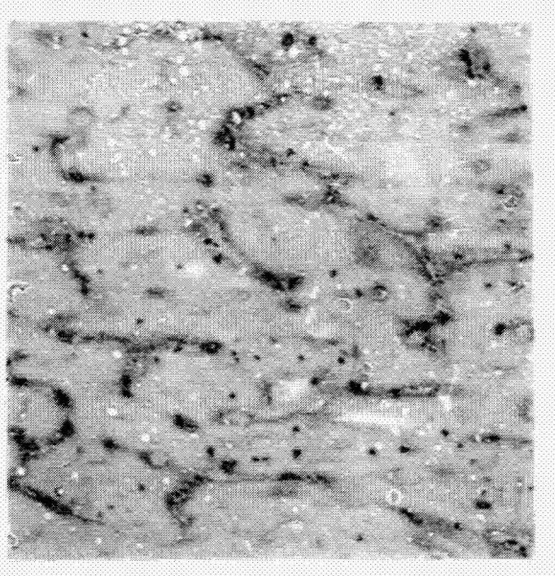

Neg. No. 53539 125X

(b)

Neg. No. 53540 125X

(c)

Figure 1. Typical optical and SEM photomicrographs of standard and modified 19-9DL alloys. (a-c) Optical, (d,e) SEM. (a) Unmodified 19-9DL (std.); (b,d) alloy code CA (2.5Ni, 0.5Al); and (c,e) alloy code CB (2.5Ni, 1Al).

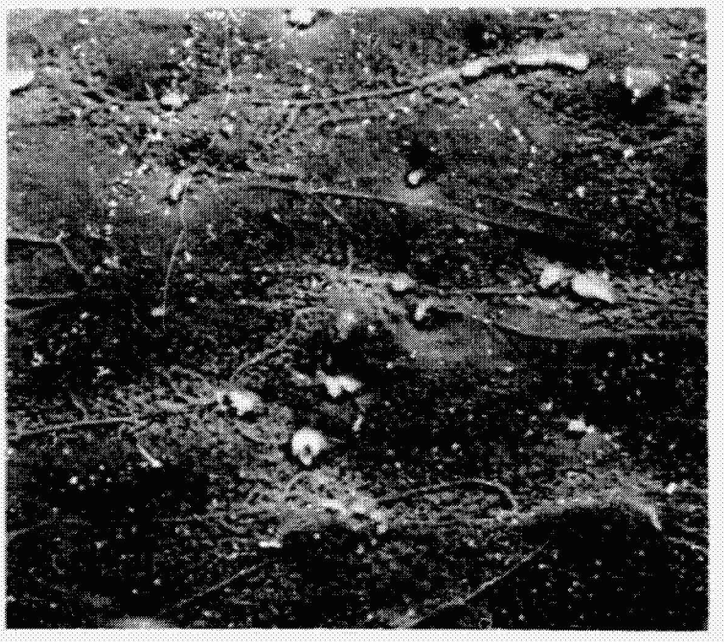

SEM No. 7582 500X

(d)

SEM No. 7585 500X

(e)

Figure 1 (cont.)

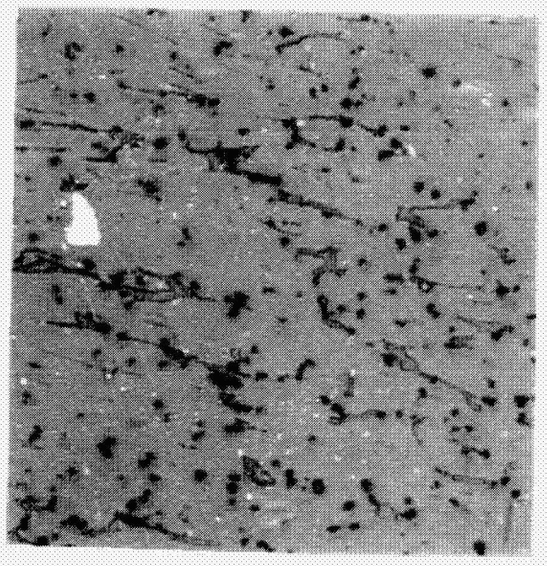

Neg. No. 53541 125X

(a)

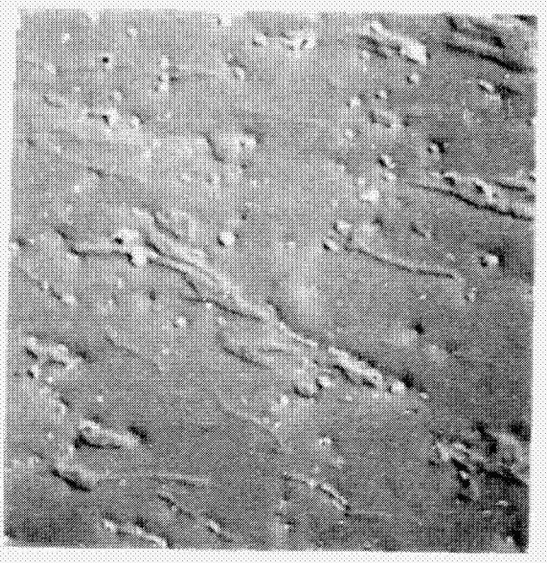

SEM No. 7598 200X

(b)

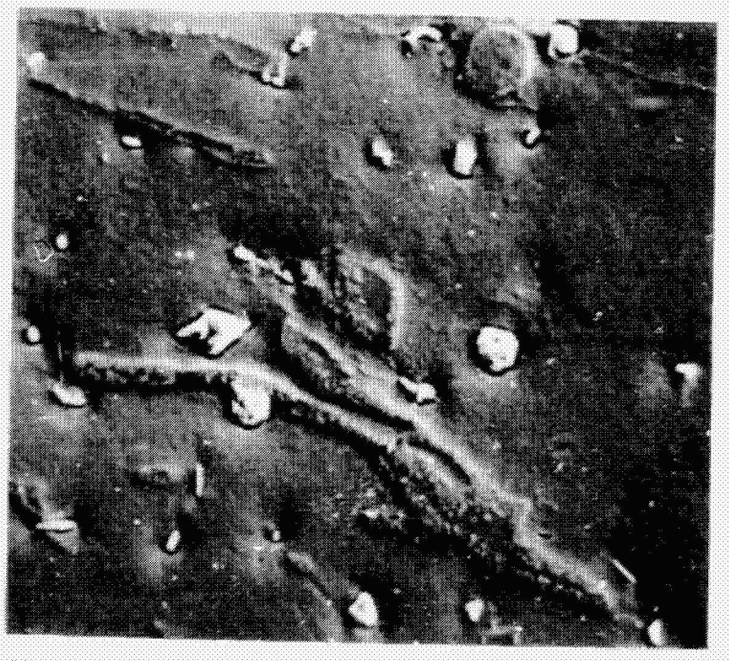

SEM No. 7599 500X

(c)

Figure 2. Optical and SEM photomicrographs showing typical microstructures of modified 19-9DL, alloy code CD (2.5Ni, 2Nb). (a) Optical; (b,c) SEM.

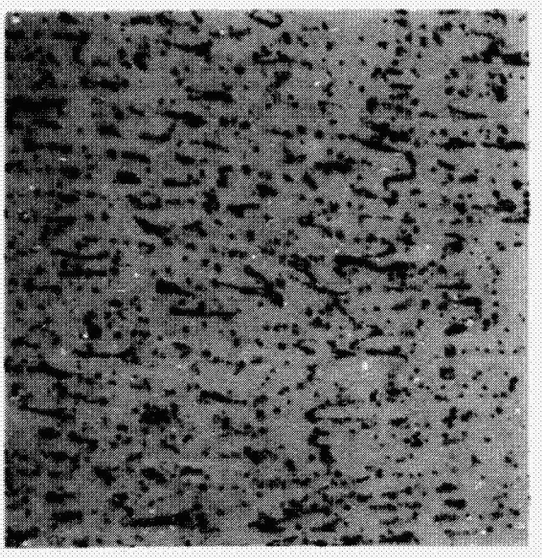

Neg. No. 53542 125X

(a)

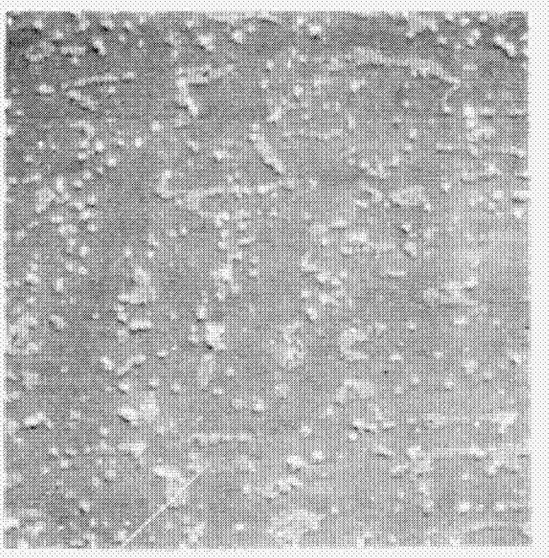

SEM No. 7587 200X

(b)

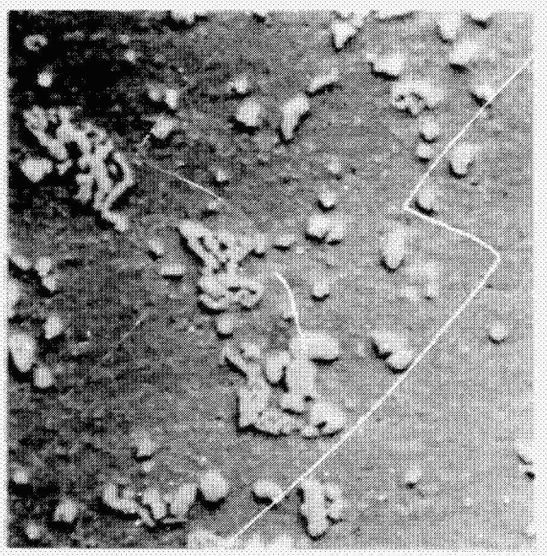

SEM No. 7588 500X

(c)

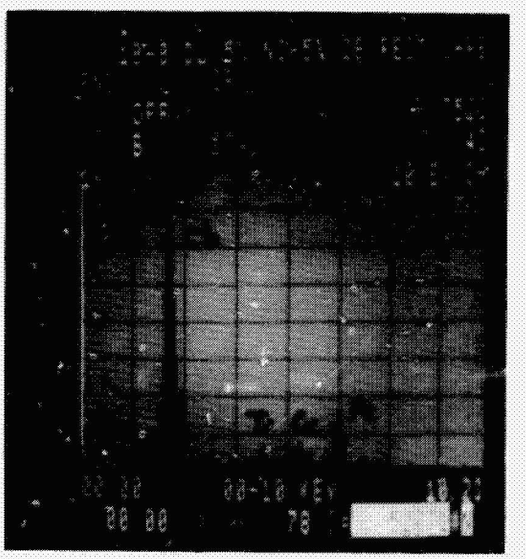

(d)

Figure 3. Optical and SEM photomicrographs and EDX from a typical area in modified 19-9DL alloy, code CE (5Ni, 5Nb). (a) Optical; (b,c) SEM; and (d) EDX from blocky particles in (c) showing high Nb and Ti.

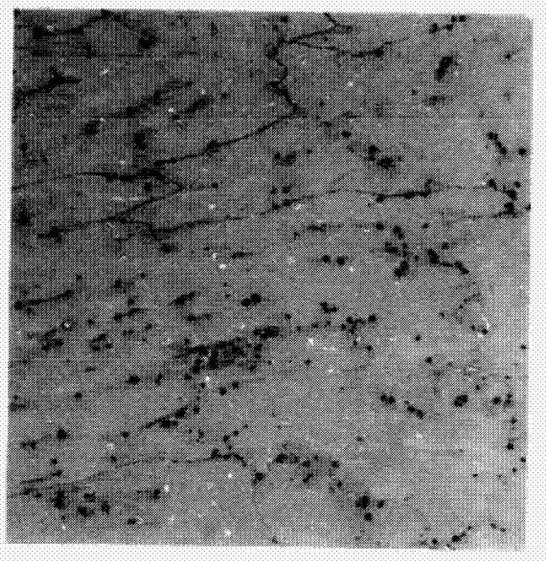

Neg. No. 53543 125X

(a)

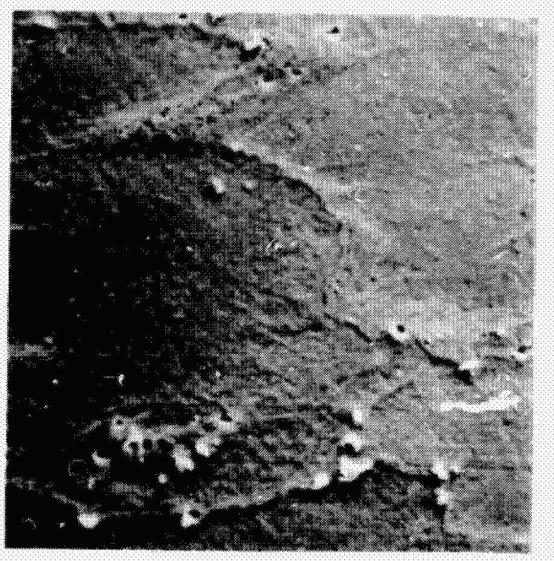

SEM No. 7590 500X

(b)

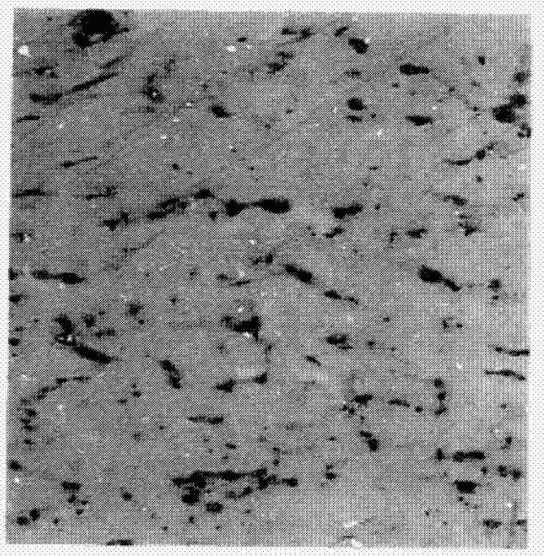

Neg. No. 53544 125X

(c)

SEM No. 7601 500X

(d)

Figure 4. Typical optical and SEM photomicrographs showing representative microstructures in modified 19-9DL alloys, codes CF (2.5Ni, 0.1 misch metal) and CG (2.5Ni, 0.3 misch metal). (a) Alloy code CF, optical; (b) alloy code CF, SEM; (c) alloy code CG, optical; and (d) alloy code CG, SEM.

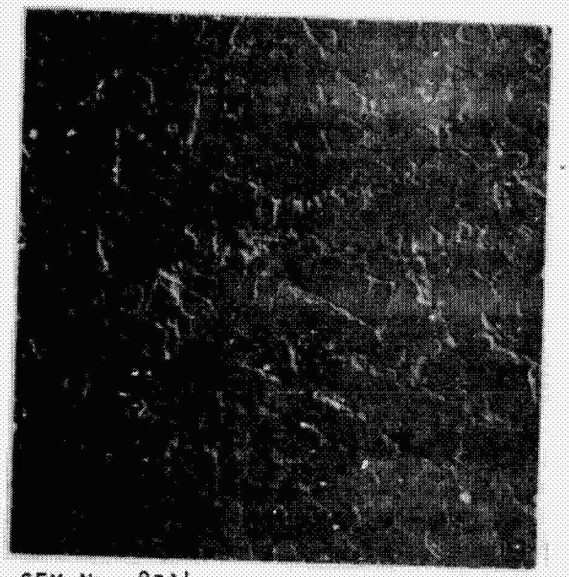

SEM No. 8314 100X

(a)

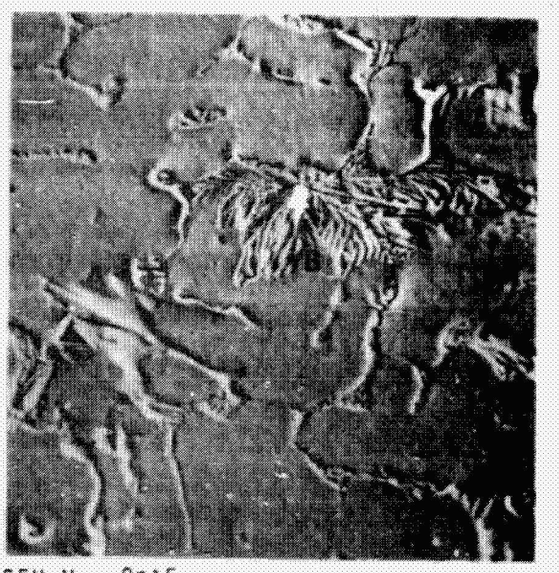

SEM No. 8315 300X

(b)

SEM No. 8316A 300X

(c)

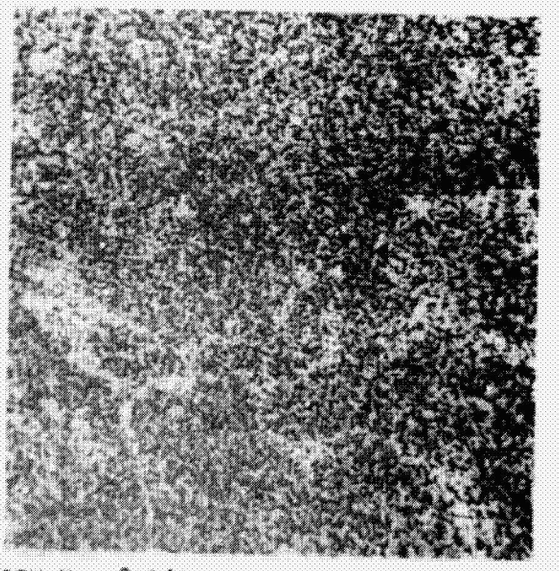

SEM No. 8316B 300X

(d)

Figure 5. SEM photomicrographs and X-ray maps of alloy CRM-6D. (a) Dendritic structure and interdendritic carbides; (b) morphology of lamellar (B) and solid-looking (A) carbides; (c) and (d) Mo and Cr X-ray maps, respectively, of (b).

SEM No. 8317 100X

(a)

SEM No. 8318 500X

(b)

SEM No. 8319 500X

(c)

Figure 6. SEM photomicrographs and X-ray map of alloy XF-818. (a) Low-magnification dendritic structure; (b) morphology of interdendritic carbides; (c) Mo X-ray map of (b).

SEM No. 8321 100X

(a)

SEM No. 8322A 500X

(b)

SEM No. 8323 100X

(c)

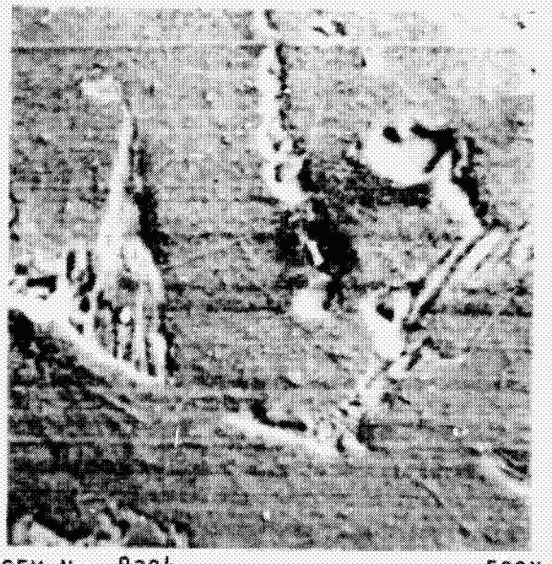

SEM No. 8324 500X

(d)

Figure 7. SEM photomicrographs of alloy SA-F11 and HS-31. SA-F11: (a) dendrites, (b) lamellar carbides. HS-31: (c) low magnification and (d) carbides.

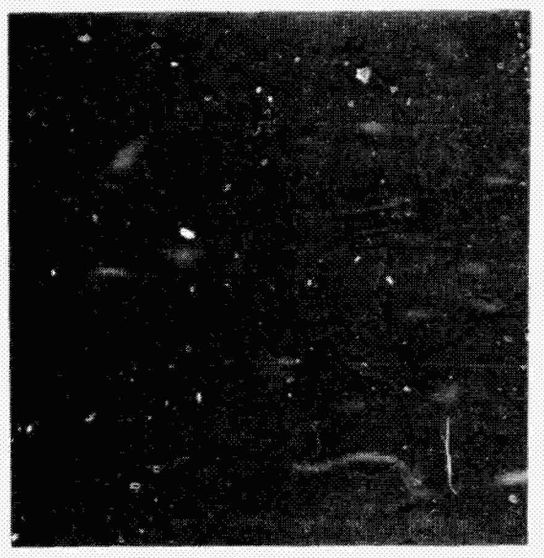

Neg. No. 55175 100X

(a)

SEM No. 1121 X2

(b)

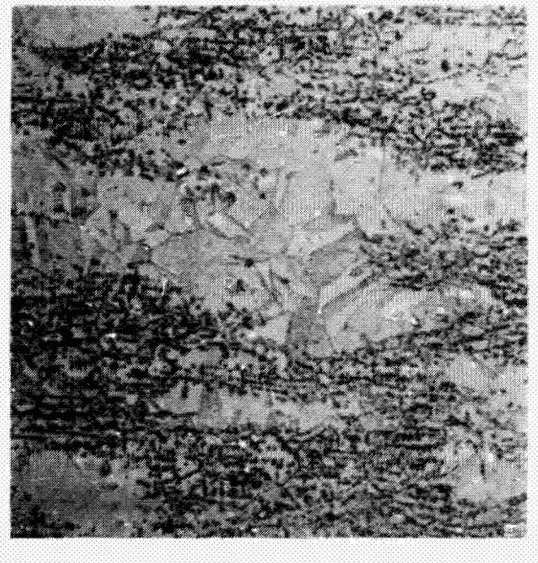

Neg. No. 55173 100X

(c)

SEM No. 1117 X100

(d)

Figure 8. Optical and SEM photomicrographs of long-range ordered alloys Ni_3Al and $(Fe,Ni)_3(V,Al)$. Ni_3Al: (a) optical, (b) SEM (backscattered); and $(Fe,Ni)_3(V,Al)$: (c) optical, (d) SEM (backscattered). Etchant: HF, H_3PO_4, HNO_3, HCl, acetic acid and water.

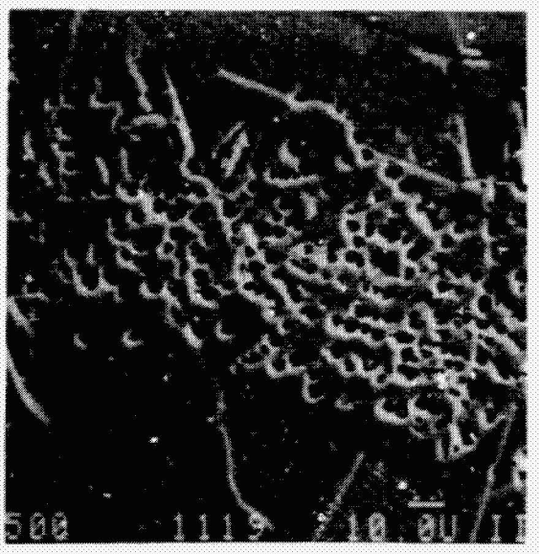

SEM No. 1119 500X

(a)

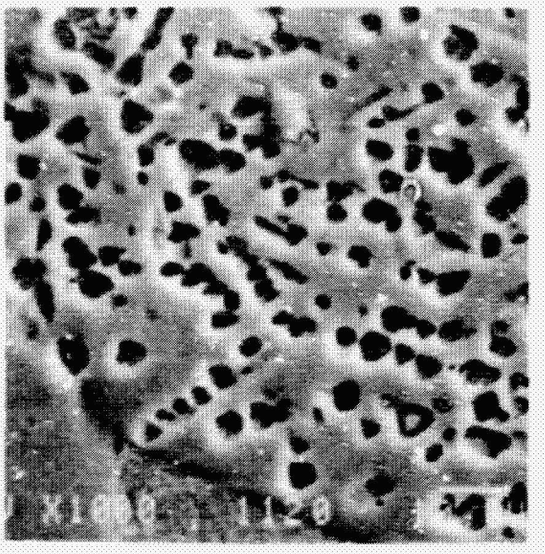

SEM No. 1120 1000X

(b)

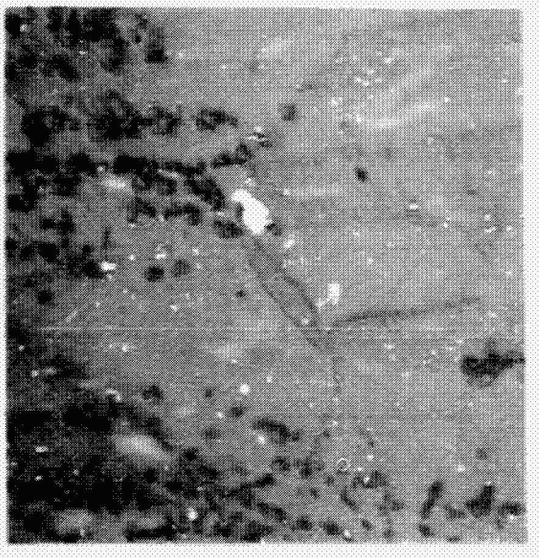

Neg. No. 55174 500X

(c)

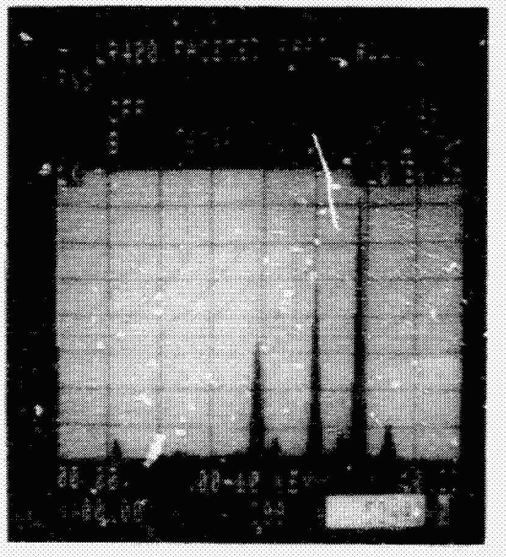

(d)

Figure 9. SEM and optical photomicrographs and EDX spectra of $(Fe,Ni)_3(V,Al)$. (a,b) SEM micrograph showing faceted and a few elongated second-phase particles in twinned matrix, (c) optical micrograph showing particle distribution, and (d) EDX spectra of a faceted particle from (b).

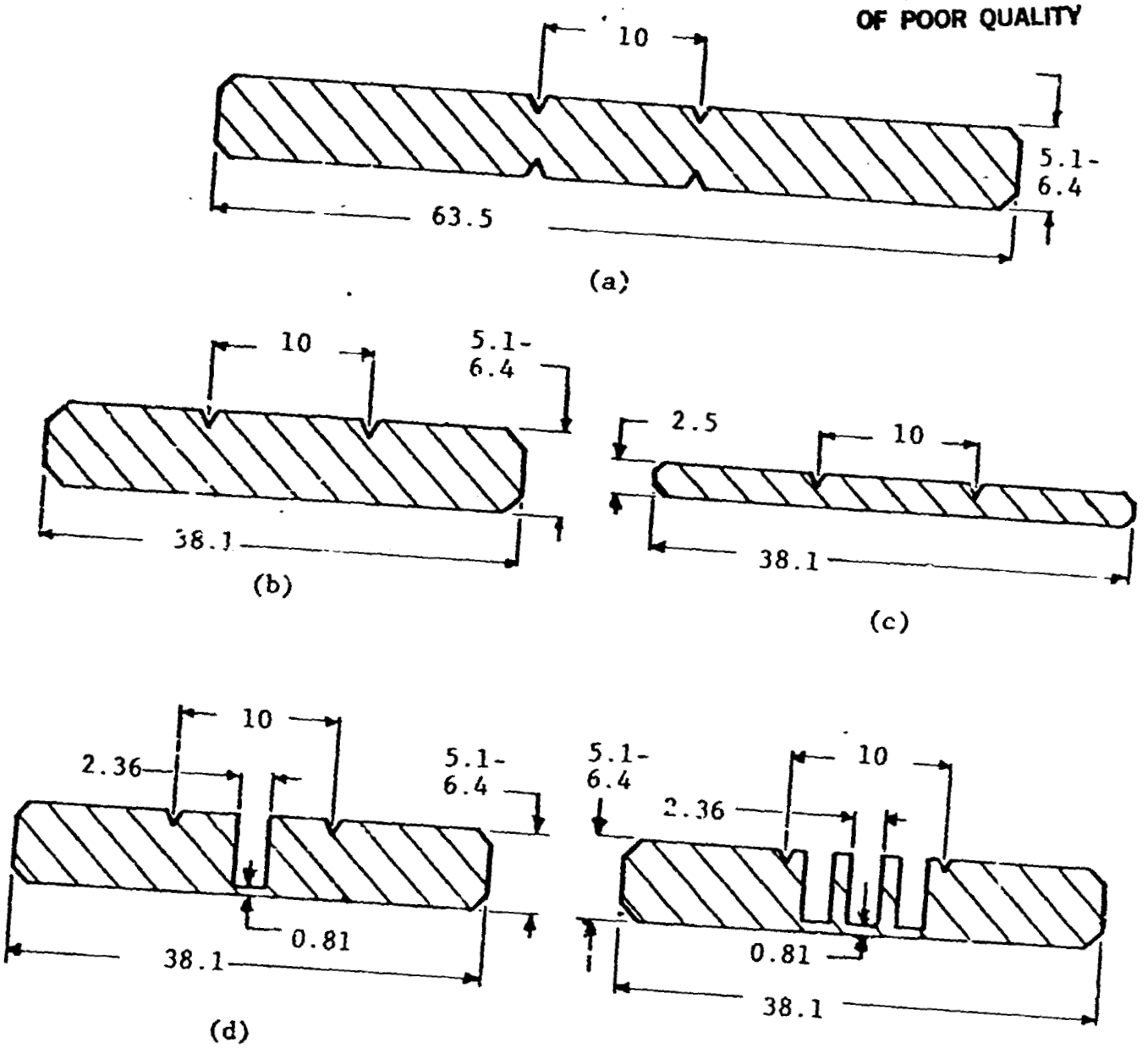

All dimensions in millimeters.

Figure 10. Different designs of hydrogen permeability specimens. (a) Initial design, (b) standard monolithic design, (c) thin specimen, (d) single cavity, and (e) multicavity, 4 or 7.

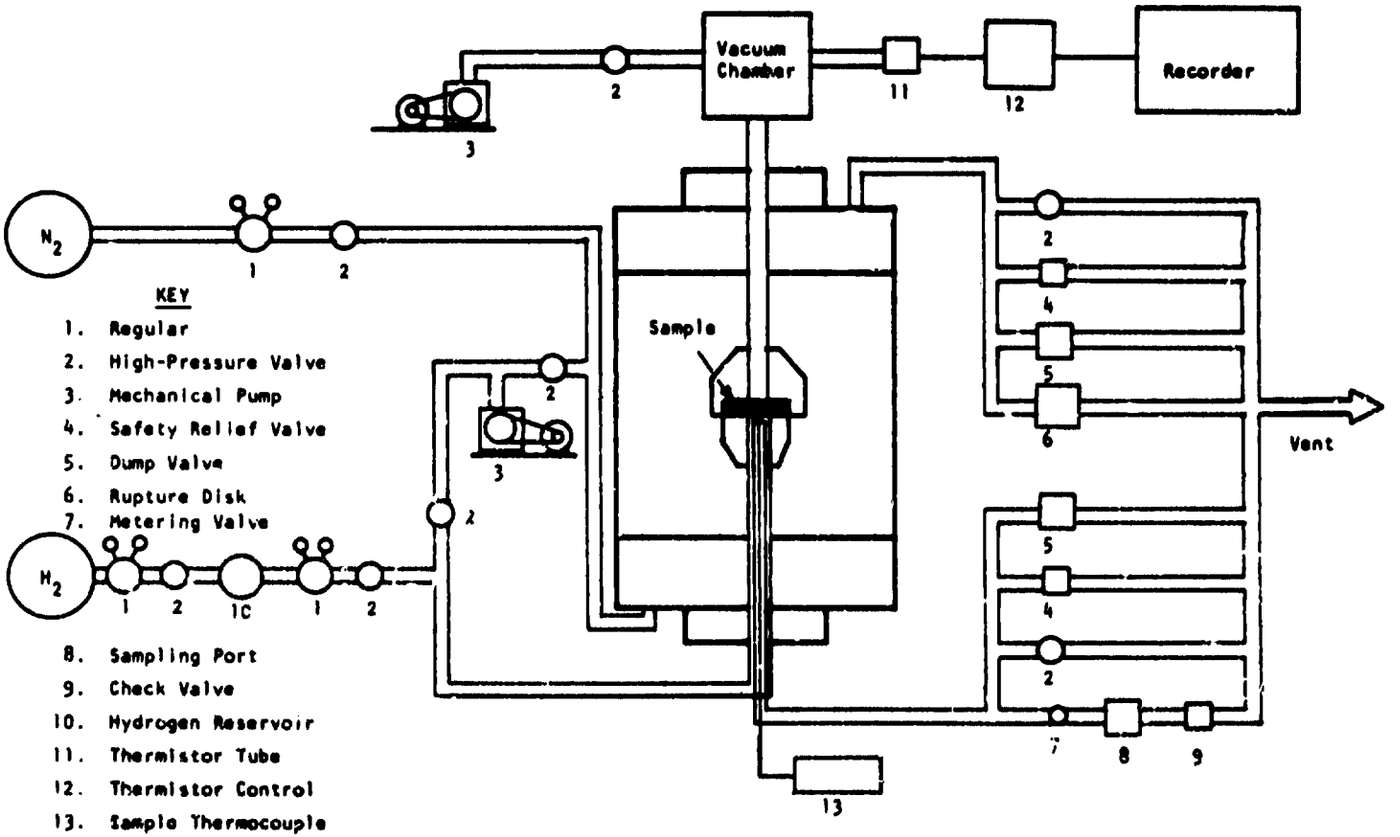

Figure 11. Schematic diagram of the high pressure-high temperature permeation system.

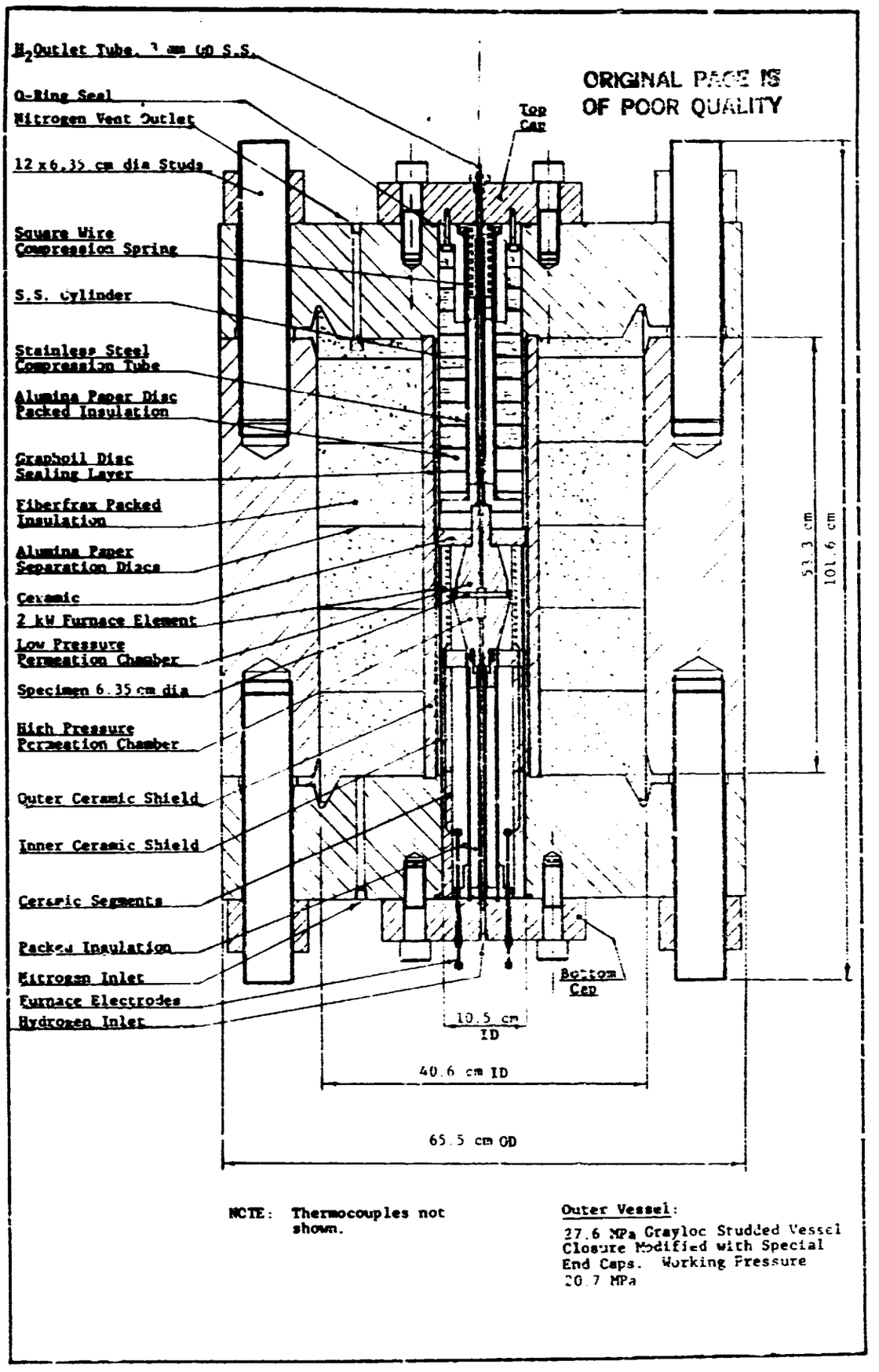

Figure 12. Design of internals of permeability test vessel.

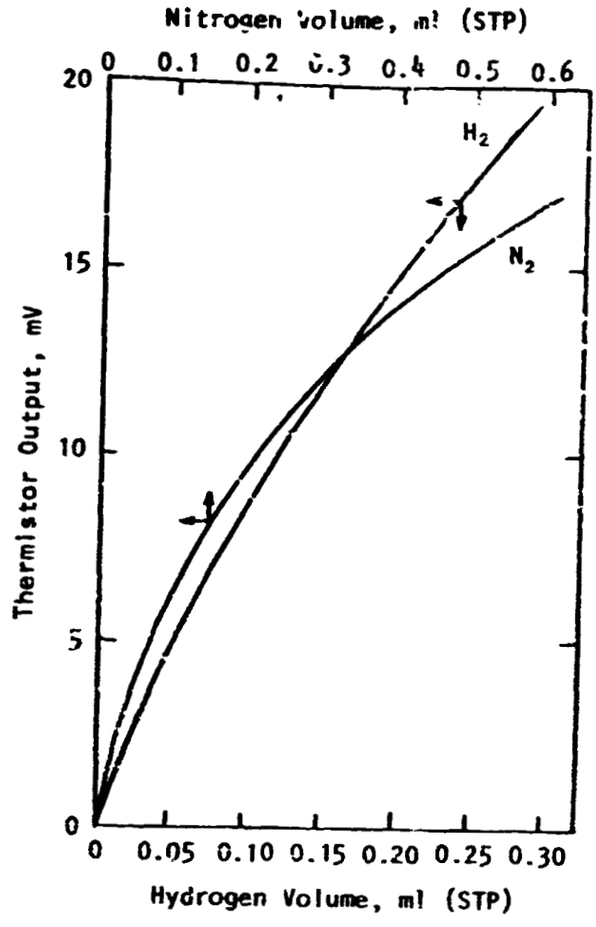

Figure 13. Calibration curve for hydrogen collection vessel/thermistor gauge system.

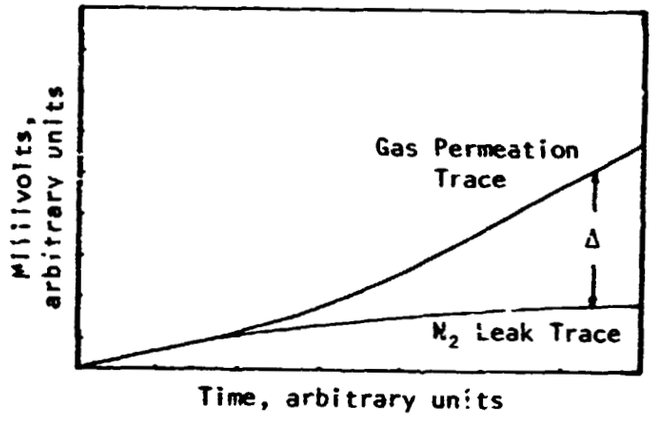

Figure 14. Schematic representation of nitrogen leak and permeation traces of chart recorder. From the difference (Δ), the net permeation was estimated.

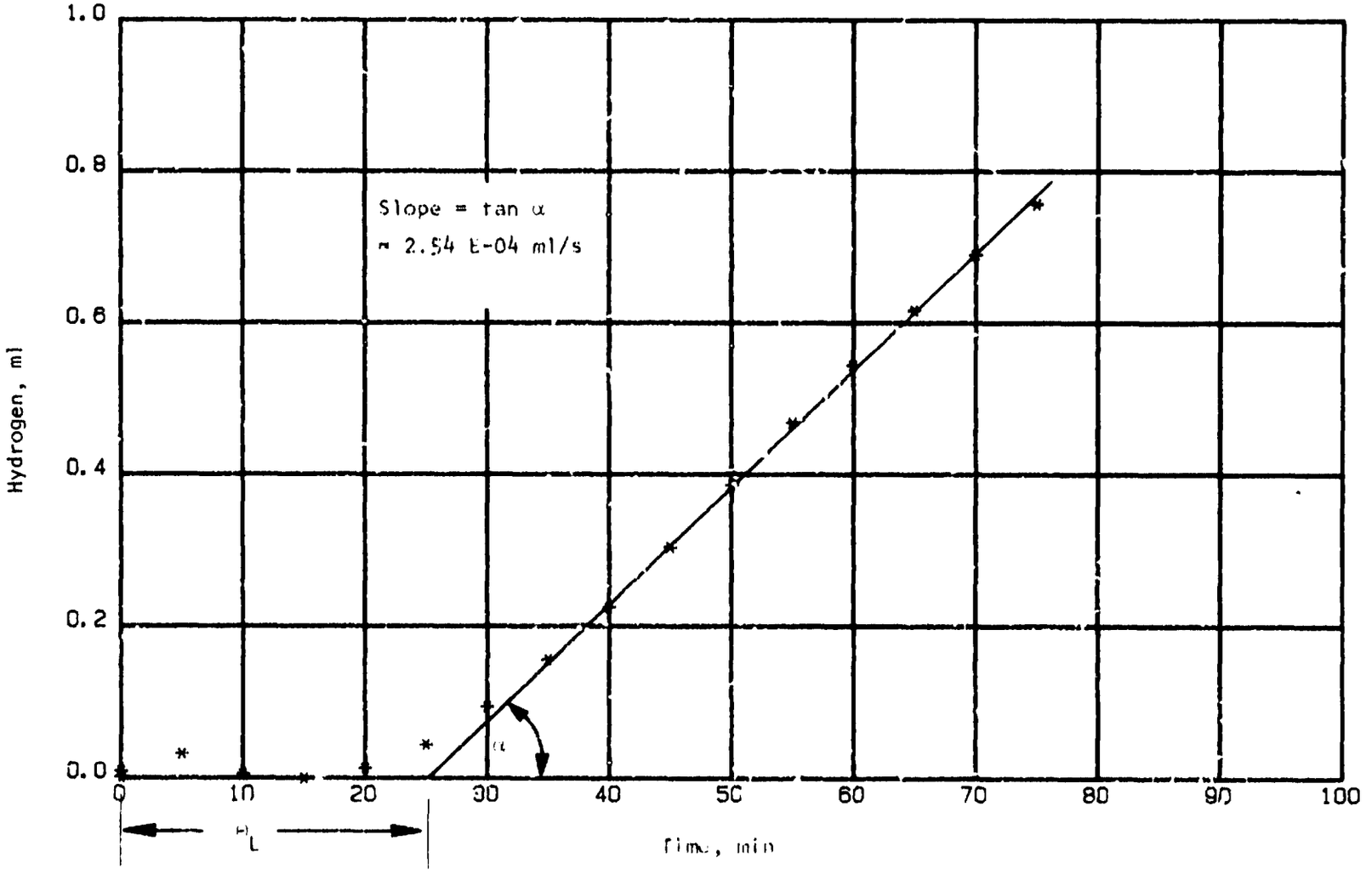

Figure 15. Plot of amount of hydrogen permeating as a function of time in pure H_2. Alloy Ni_3Al at 870°C.

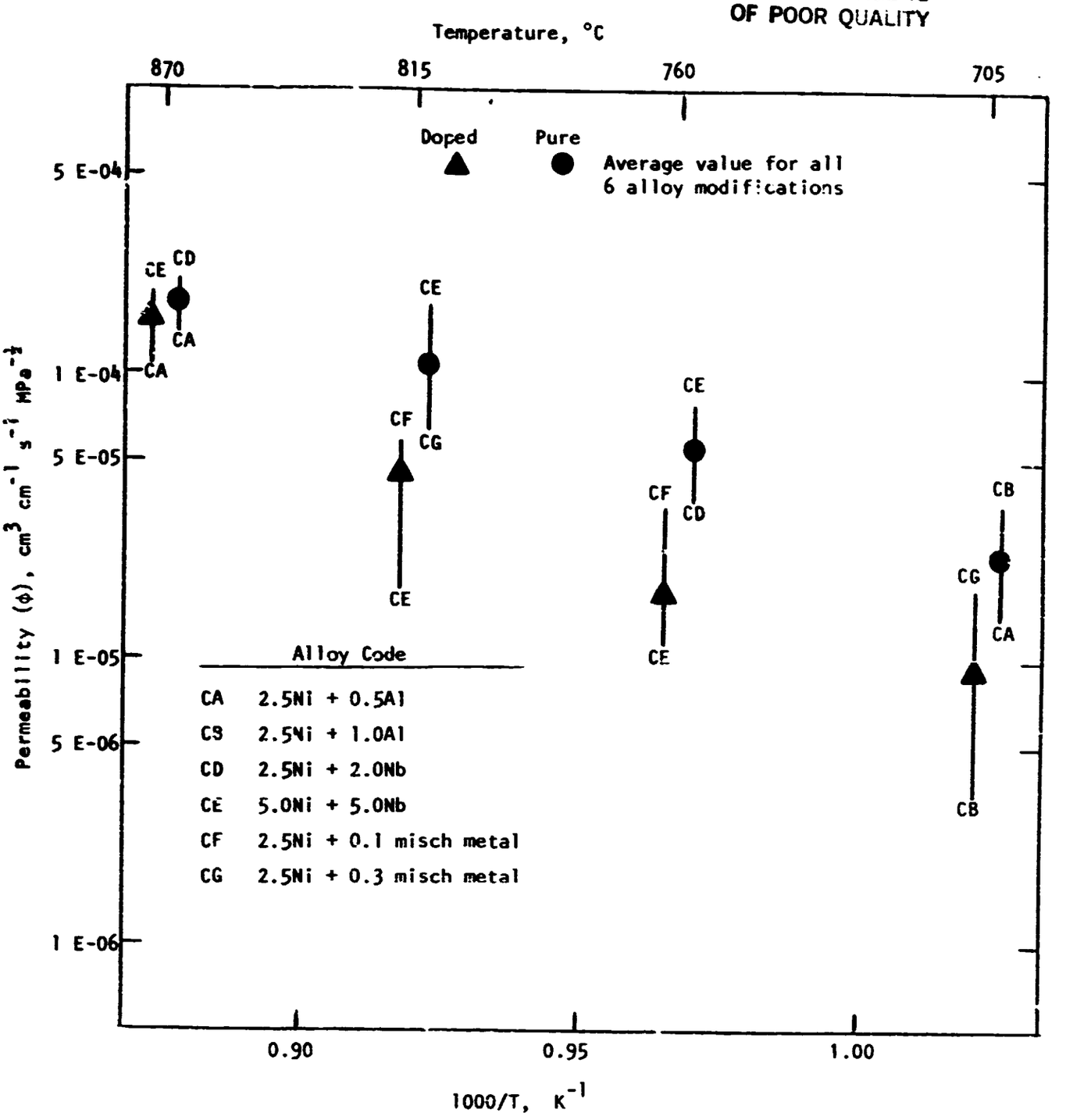

Figure 16. Effect of temperature on hydrogen permeability in six modified 19-9DL alloys in pure and 1% CO_2-doped hydrogen (Task VIII).

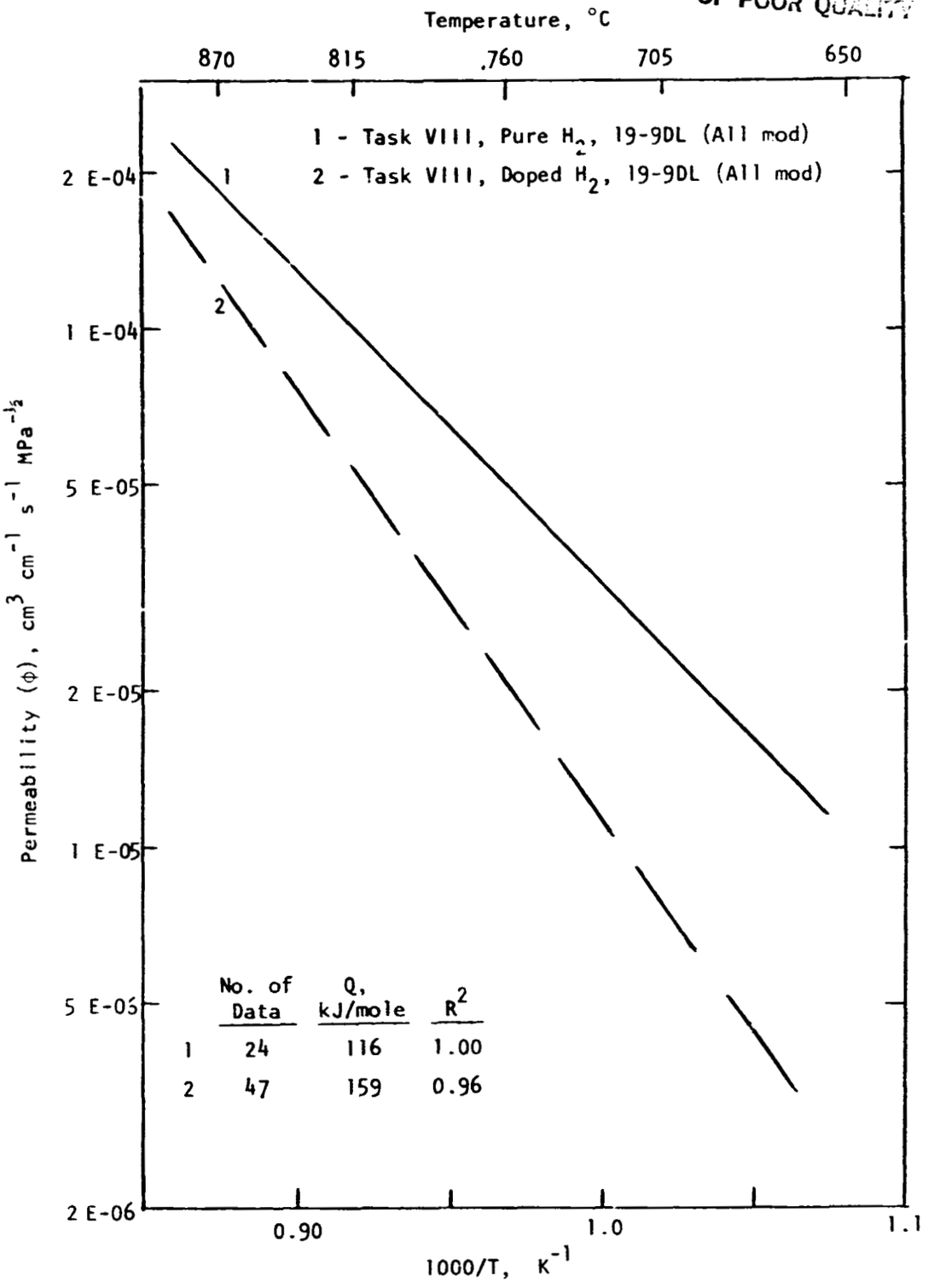

Figure 17. Effect of temperature on hydrogen permeability in modified 19-9DL alloys, in pure H_2 and in H_2 with 1% CO_2.

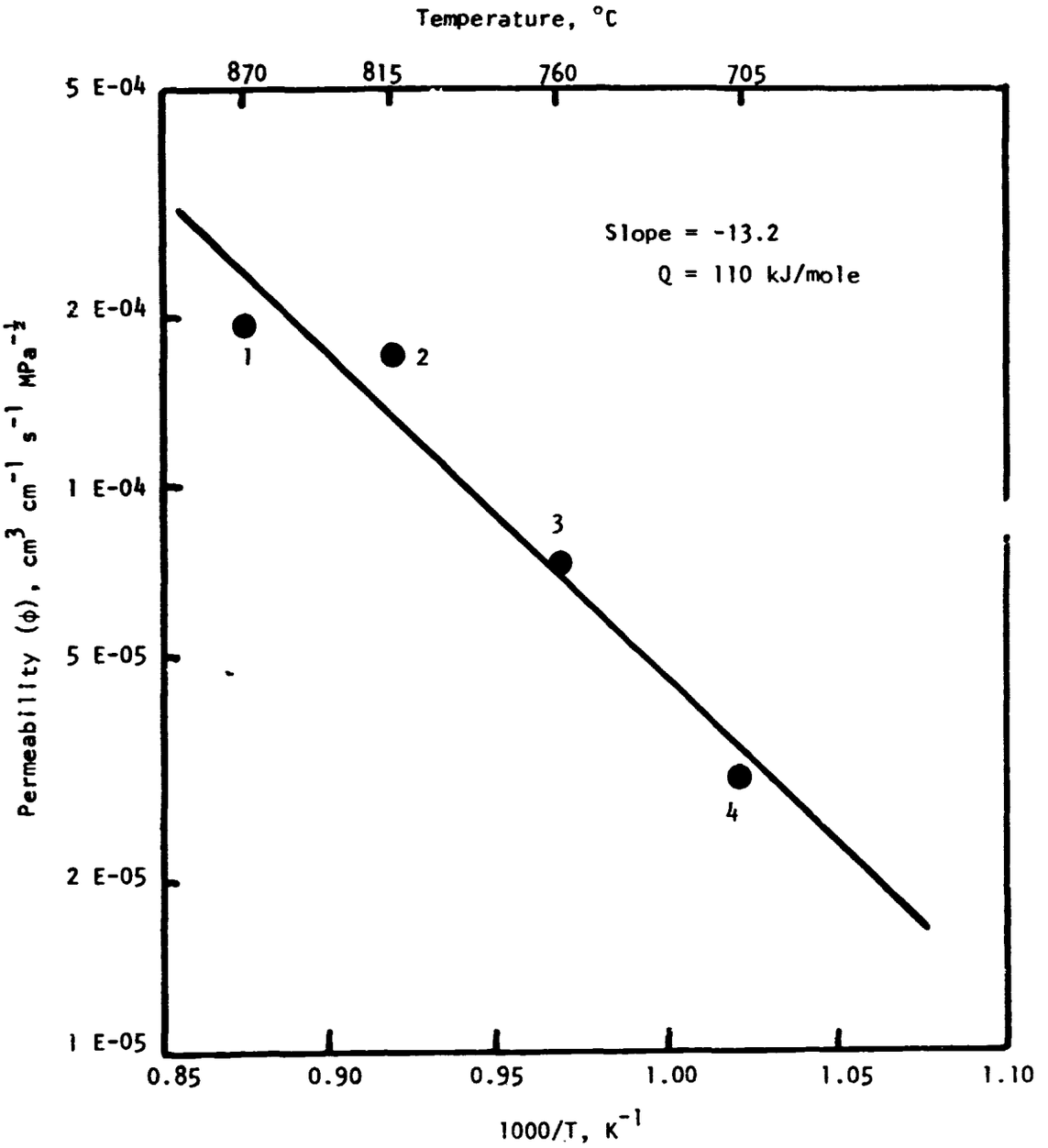

Figure 18. Effect of temperature on hydrogen permeability in modified 19-9DL (5% Ni, 5% Nb) in pure H_2 environment (test 97).

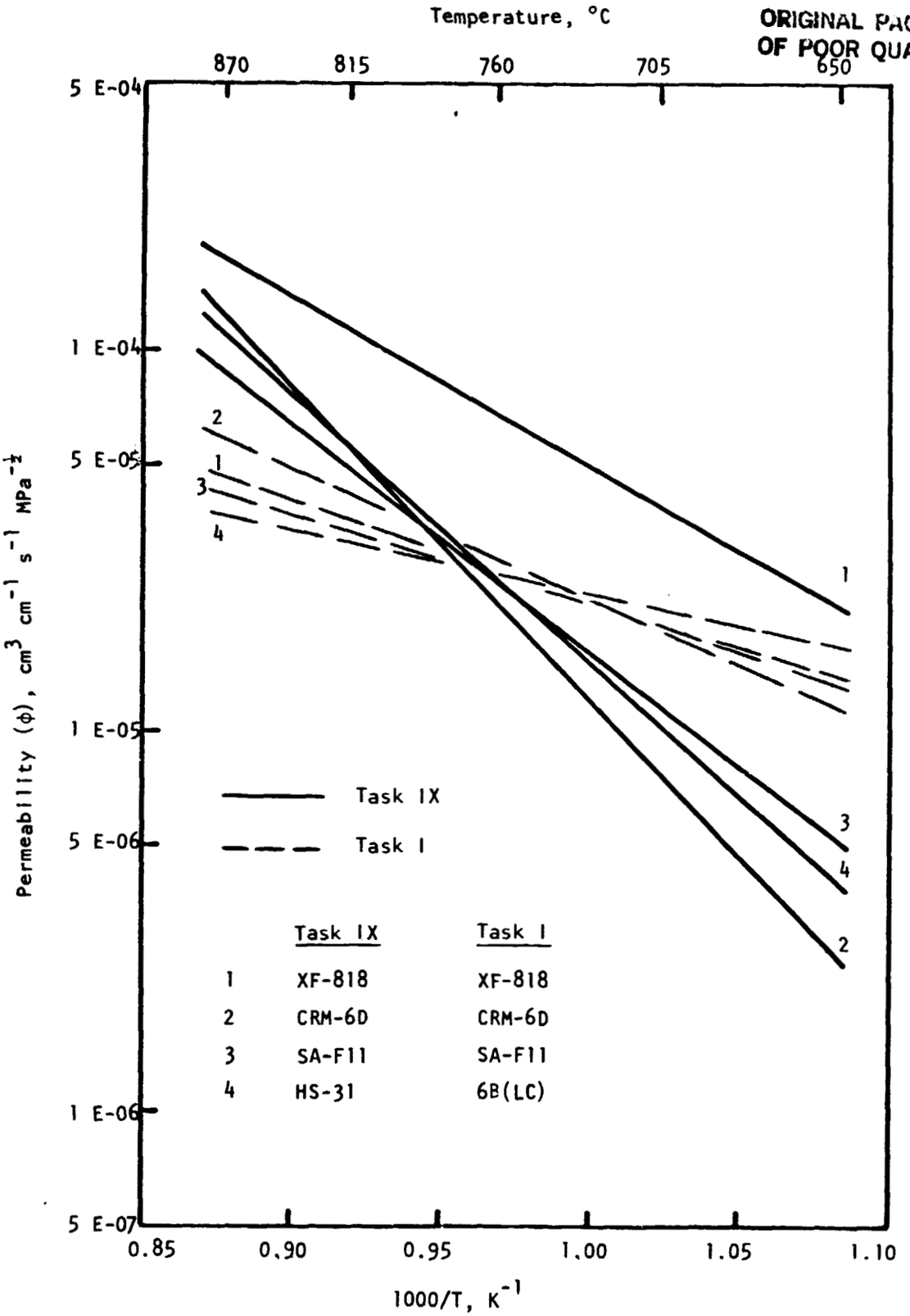

Figure 19. Effect of temperature on permeability in high-temperature alloys in pure H_2 environment (Task IX).

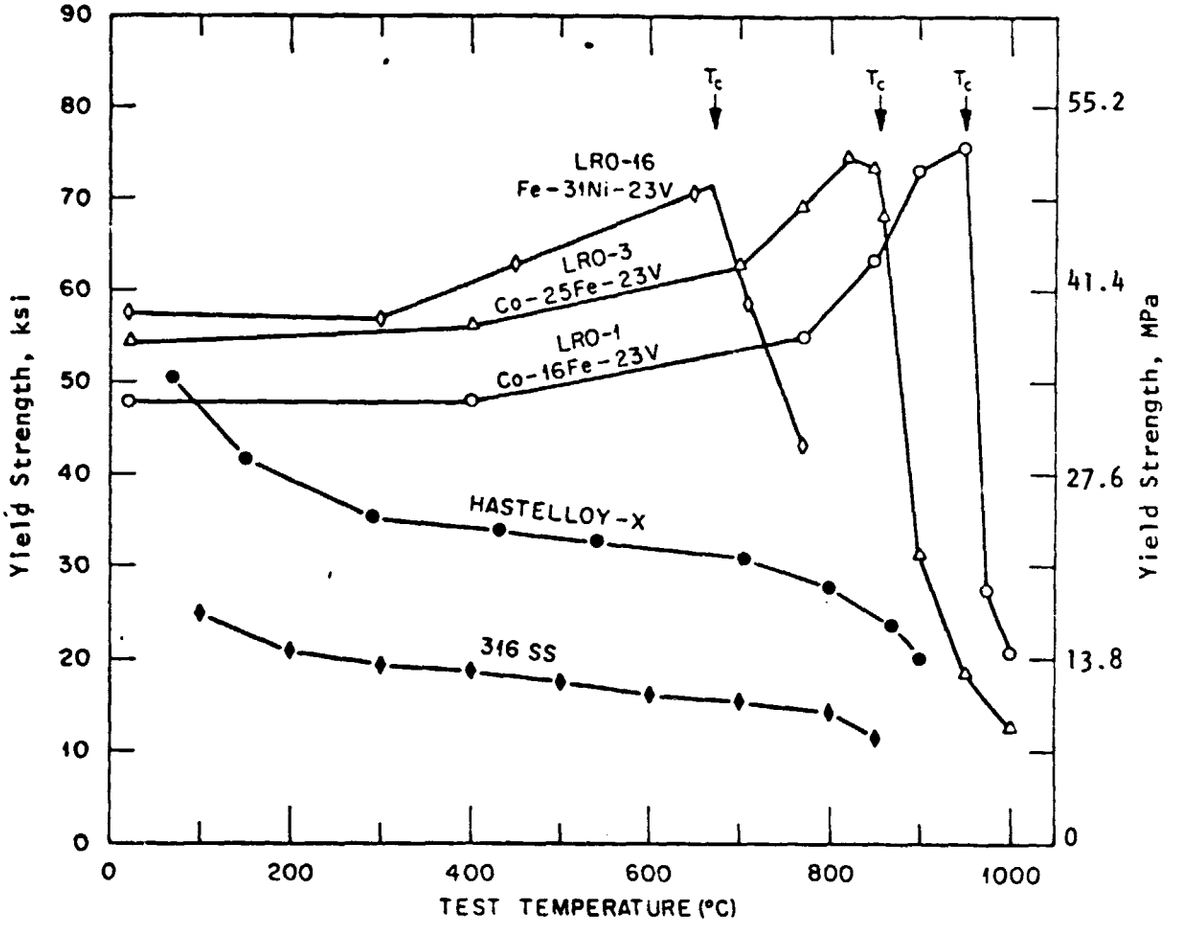

Figure 20. Effect of temperature on yield strength of long-range ordered alloys.[5] *T_c = critical ordering temperature.*

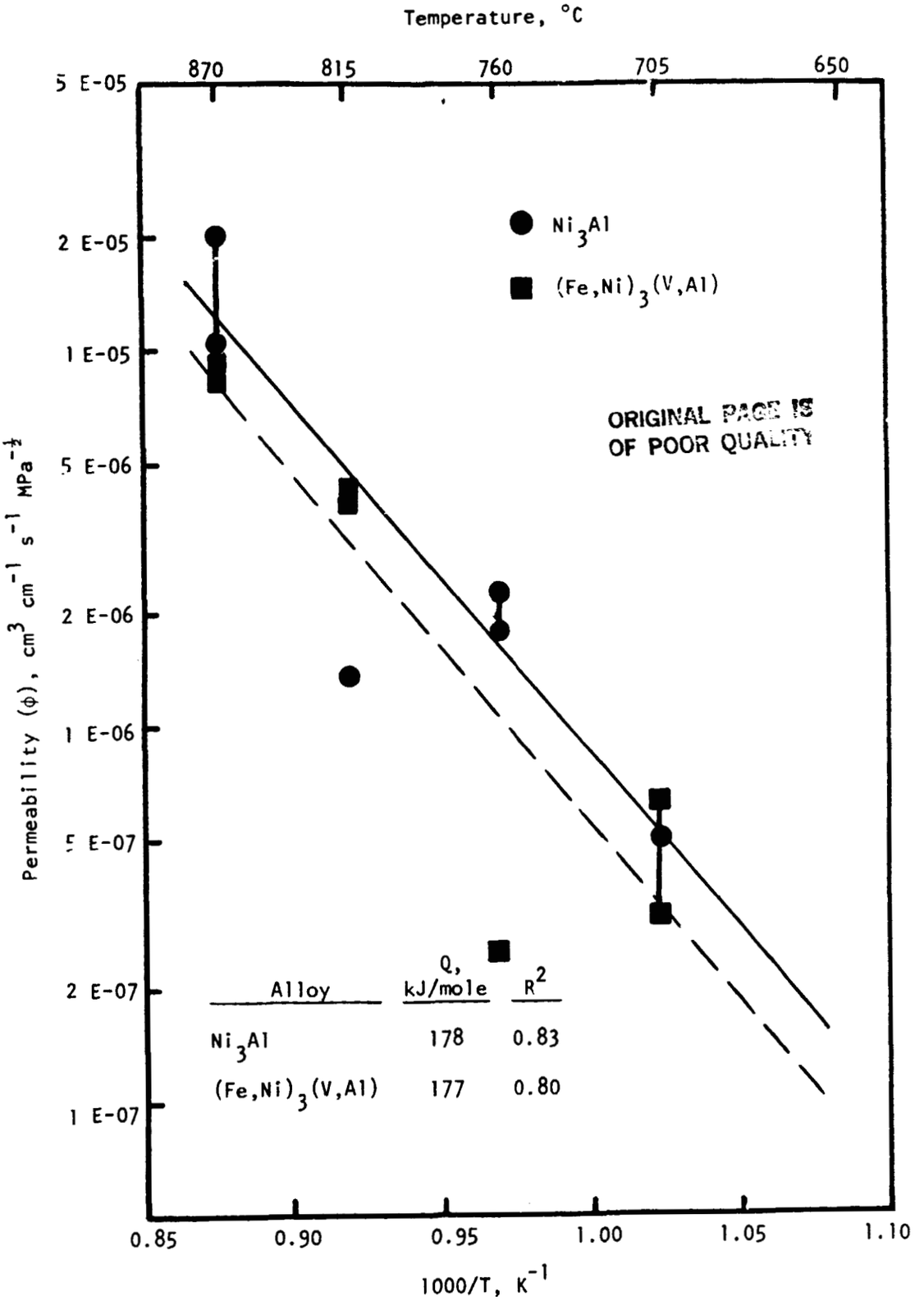

Figure 21. Effect of temperature on permeability in long-range ordered alloys, Ni_3Al and $(Fe,Ni)_3(V,Al)$ in pure H_2 (Task X).

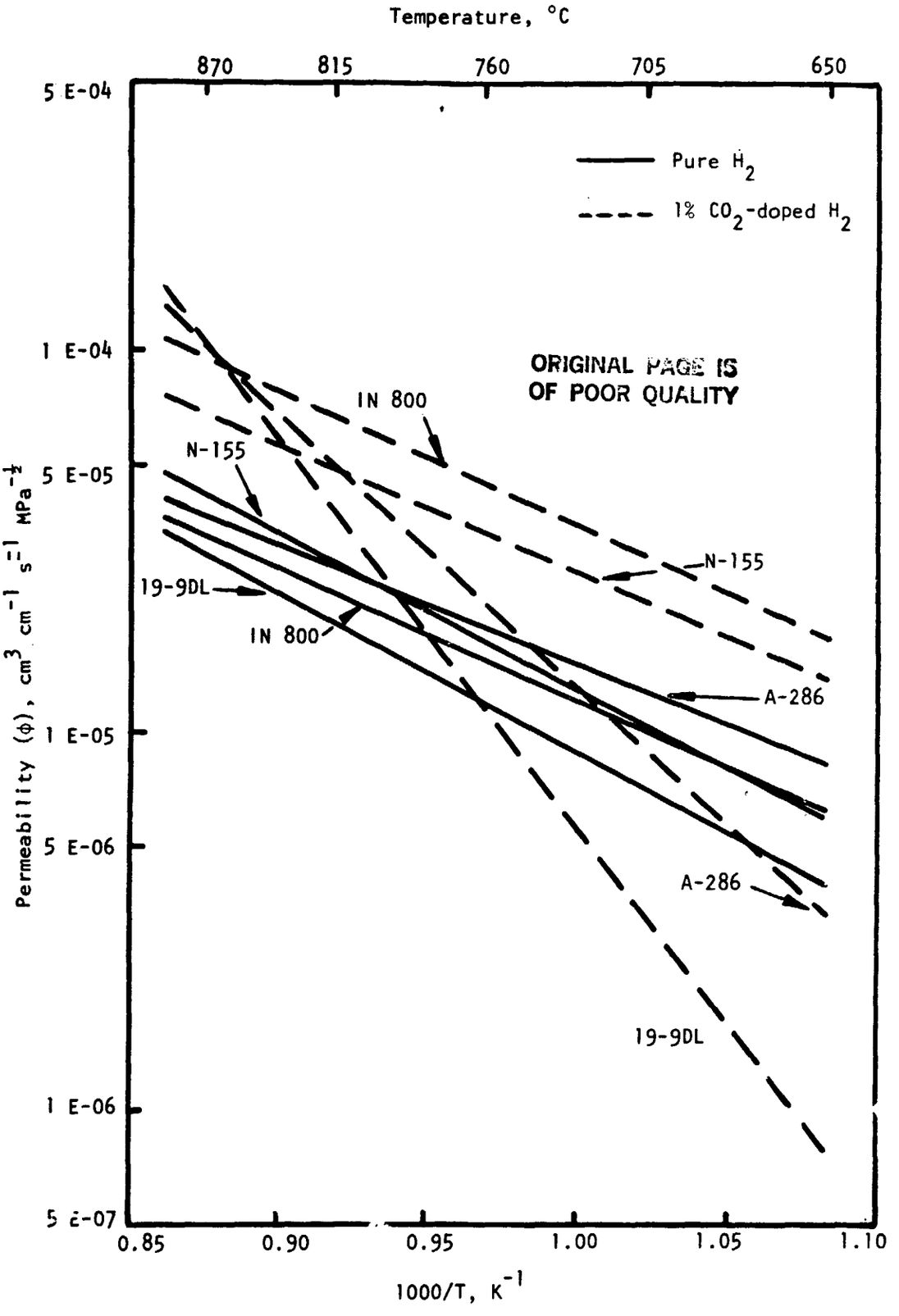

Figure 22. Effect of temperature on permeability in commercial N-155, 19-9DL IN 800, and A-286 in pure (Task I) and 1% CO_2-doped H_2 (Task VII).

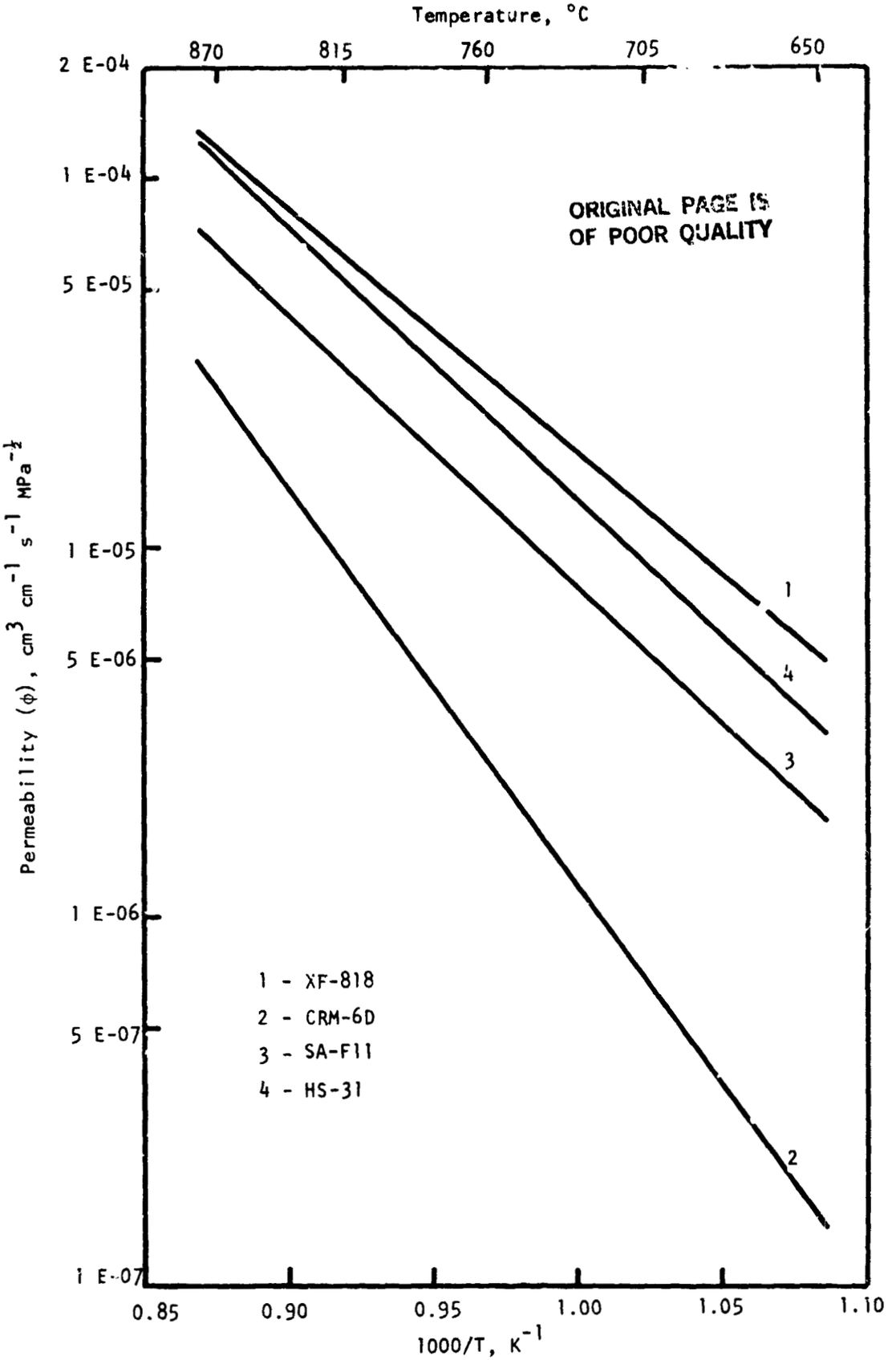

Figure 23. Effect of temperature on H_2 permeability in high-temperature alloys in 1% CO_2-doped H_2 (Task IX).

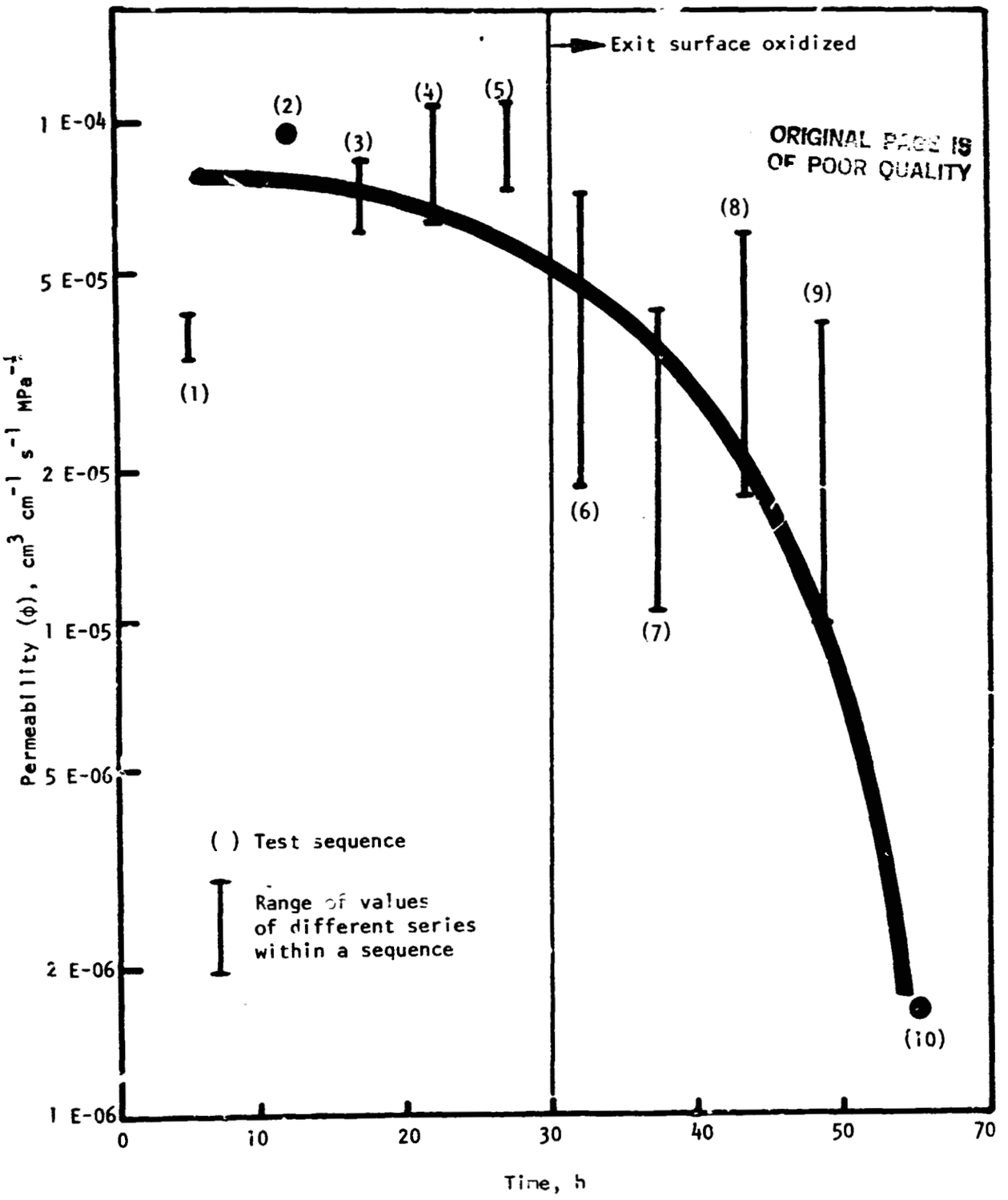

Figure 24. Effect of exit surface oxidation on H_2 permeability in IN 800 at 815°C, 5.96 mm thick specimen, 1% CO_2 + H_2 (test 71).

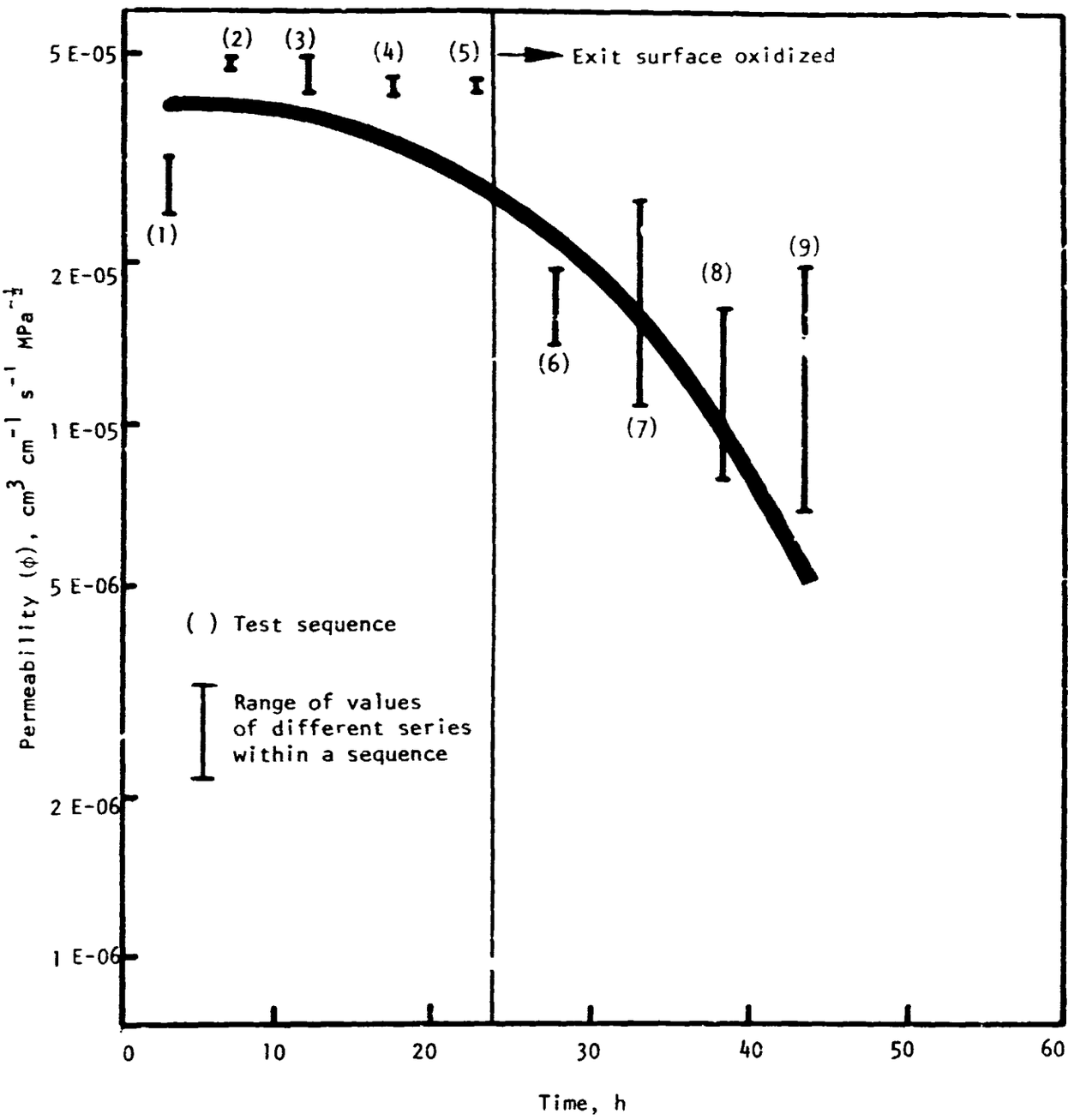

Figure 25. Effect of exit surface oxidation on H_2 permeability in IN 800 at 815°C, 2.65 mm thick specimen, 1% CO_2 + H_2 (test 72).

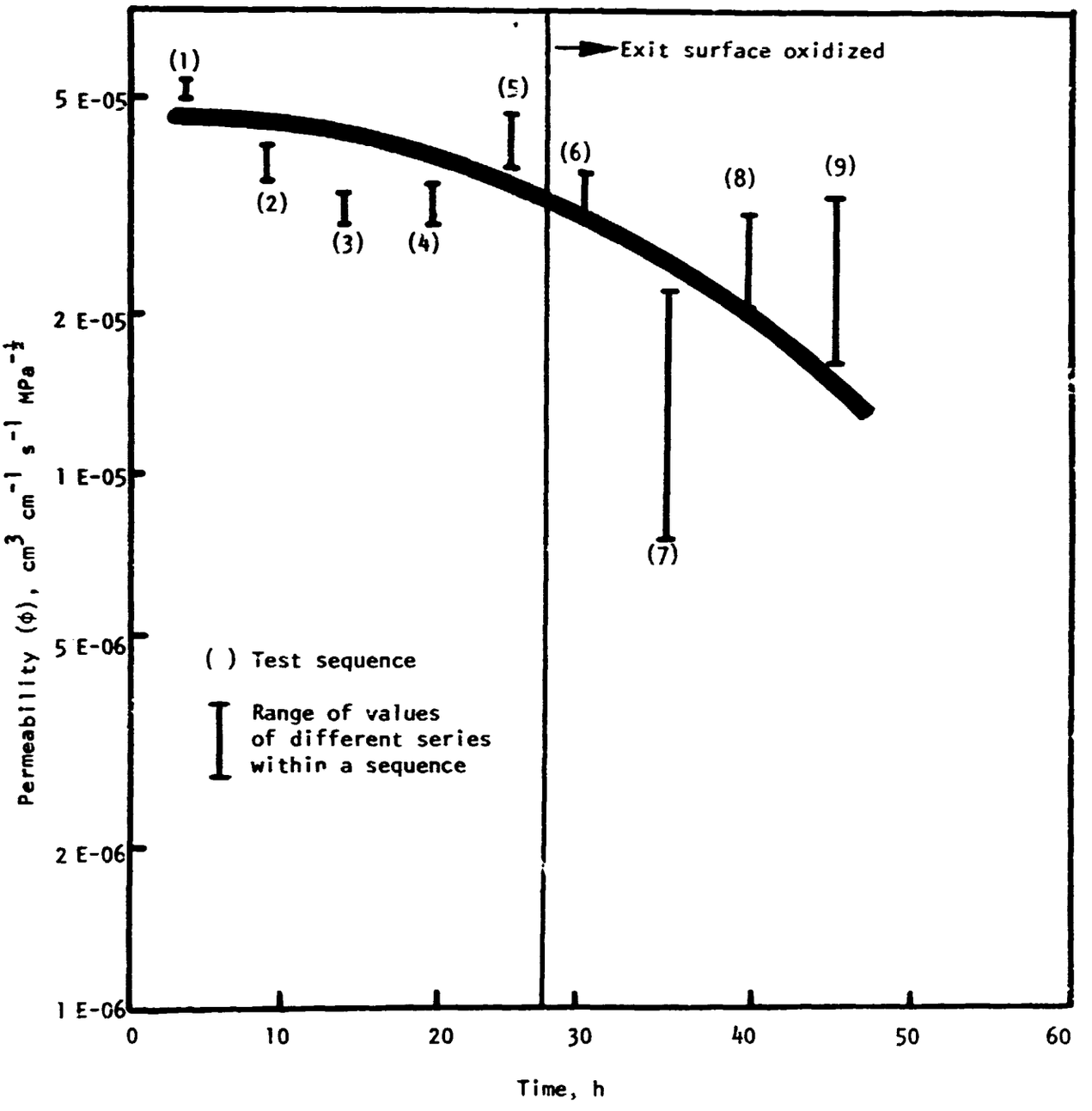

Figure 26. Effect of time on H_2 permeability in IN 800 at 815°C, 2.65 mm thick specimen, pure H_2 (test 73).

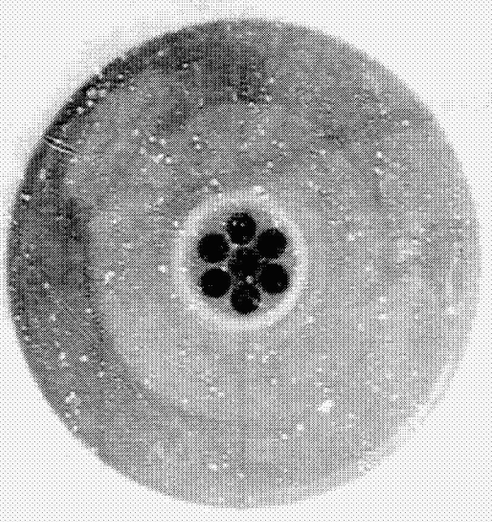

Neg. No. 53151 1.8X

(a)

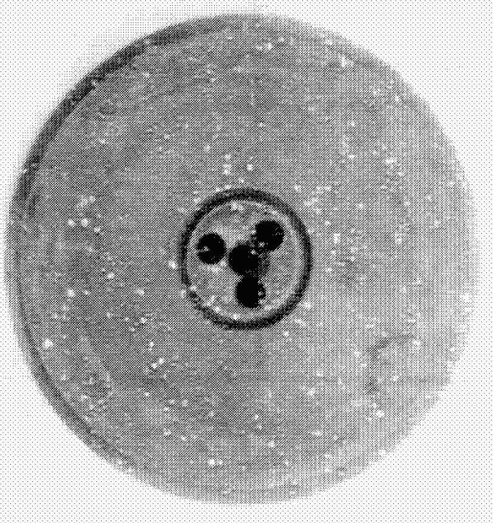

Neg. No. 53154 1.8X

Figure 27. Appearance of typical multicavity specimens. (a) Test 79, (b) test 80.

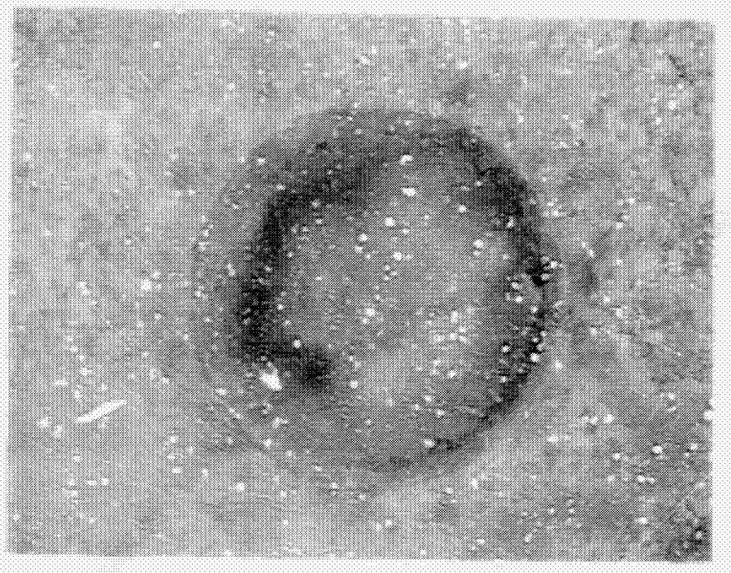

Neg. No. 53155 4X

(a)

SEM No. 6511 1000X

(b)

Figure 28. Effect of high pressures on surface features. (a) Deformation caused by hydrogen pressure in A-286 specimen (test 79); (b) cracking in surface scale inside the cavity (tension side) in 19-9DL specimen (test 78).

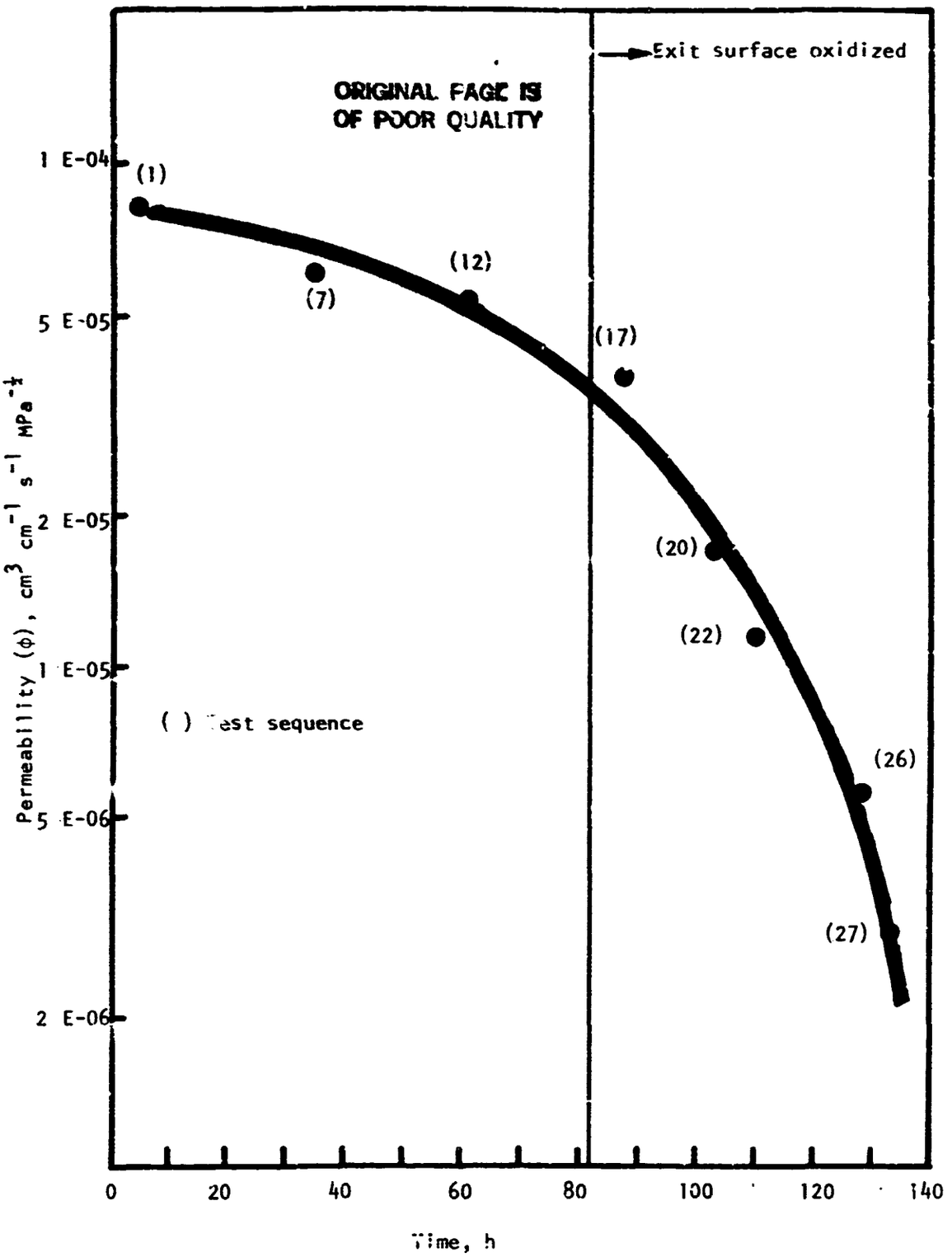

Figure 29. Effect of time on H_2 permeability in IN 800 at 815°C, 5.9 mm thick specimen, 1% CO_2-doped H_2 (test 68).

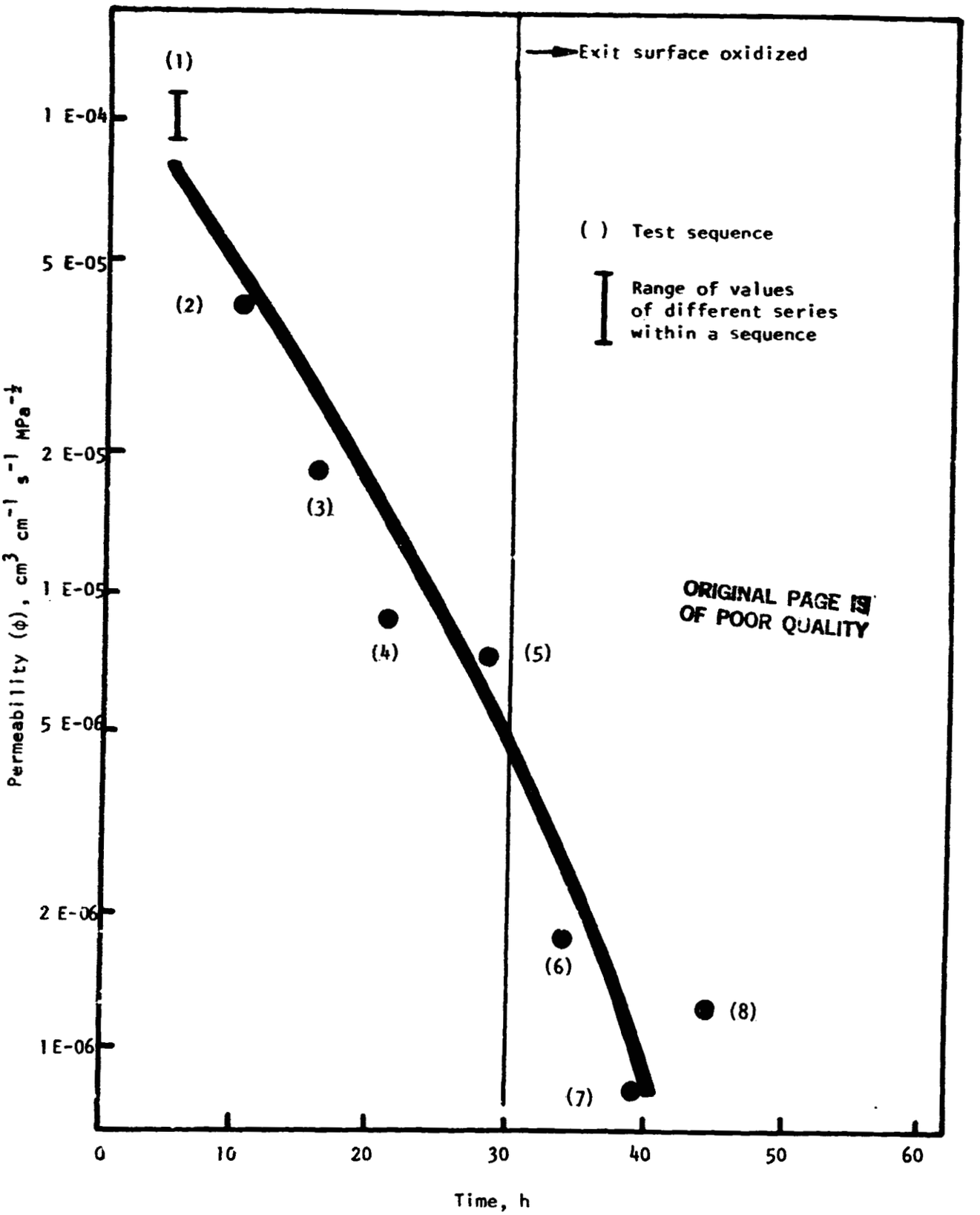

Figure 30. Effect of time on H_2 permeability in IN 800 at 815°C, 0.89 mm thick specimen, 1% CO_2-doped H_2 (test 75).

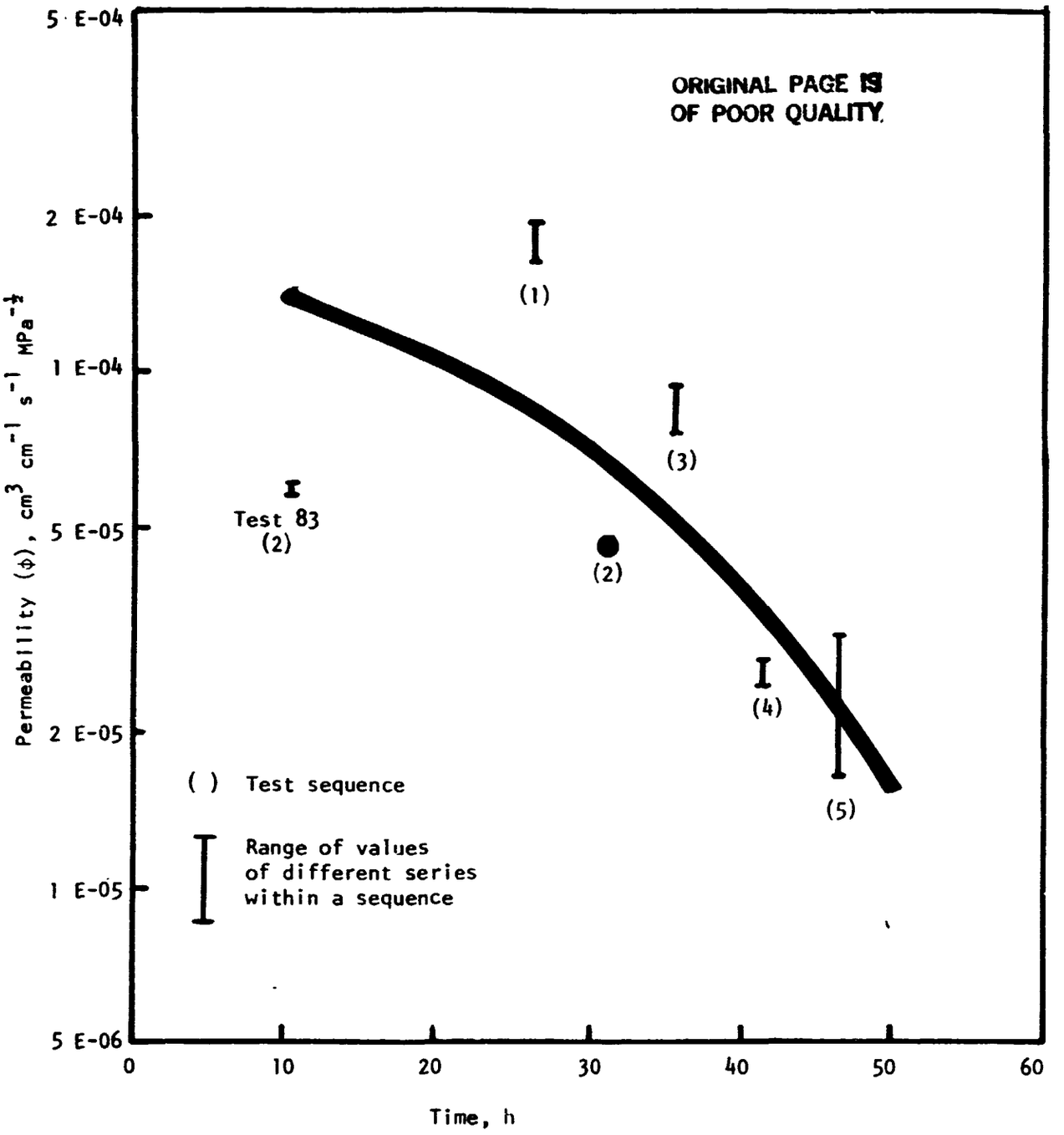

Figure 31. Effect of time on H_2 permeability in modified 19-9DL (1% Ni + 1% Al), 815°C, 0.76 mm thick specimen, 1% CO_2-doped H_2 (test 111).